MACH'S PRINCIPLE, MASS FLUCTUATIONS, AND RAPID SPACETIME TRANSPORT

James F. Woodward and Thomas L. Mahood
California State University Fullerton
Fullerton, California 92634

Abstract: The argument that Mach's principle and relativistic gravity lead to the expectation of transient fluctuations in the rest masses of objects when they are accelerated by external forces is briefly recapitulated. In appropriate circumstances such mass fluctuations can be employed to produce stationary forces (notwithstanding that in some frames of reference one may think such forces cancelled by other forces). A torsion pendulum experiment designed to search for such stationary forces is described. Small forces with the signatures expected were found. Tests of other causes that the signals might be attributed to are presented. These tests seem to rule out spurious effects as the source of the signals seen. Whether the forces seen can be brought to practical levels for rapid spacetime transport with clever engineering remains an open question.

1. Mach's Principle and Mass Fluctuations:

Mach's principle [first stated by George Berkeley nearly 200 years before Mach] is the assertion that the inertial reaction forces experienced by massive objects, when they are accelerated by external forces, are generated by the action of chiefly the most distant matter in the cosmos. Since the only known force with universal coupling to mass is gravity, it is natural to assume that, if the principle is correct, the gravitational interaction is the source of inertial reaction forces. This is in fact true in general relativity theory for the class of cosmological models thought to encompass our reality. About a decade ago, one of us realized that if inertial reaction forces are gravitational, as suggested by Mach's principle, and special relativity theory applies locally (as it does in general relativity theory), then there is reason to expect that when massive objects are accelerated, they should experience transient variations in their restmasses (Woodward, 1990). This argument was refined over the ensuing five years, appearing in final form in "Making the Universe Safe for Historians" (*i.e.*, MUSH, Woodward, 1995). That argument, with all of the mathematical steps worked out explicitly and explanatory details not previously published included, is also to be found in Appendix 2 of (Mahood, 1999). Here we merely sketch the main features of the argument.

Consider a material "test body" that is accelerated by the action of some external force. It experiences an inertial reaction force that acts on the accelerating agent. This force is the gravitational force due to the distant matter in the cosmos. We assume that the force is a relativistically invariant "four-force" which has a "time-like" part in addition to the usual three spatial components of forces. The time-like part of four-forces turn out to be the rates at which the forces create energy in the test body, that is their powers. (See W. Rindler's outstanding book [1991] on this matter, especially pages 90 and 91.) To express the inertial reaction force in terms of the field that produces it, we divide the force by the mass of the test body to get the force per unit charge. The resulting expression is further modified by translating the mass [*i.e.*, gravitational charge] into a density, since field equations relate field strengths to the local density of sources. Then, just as one gets the equation for the electric field by taking the divergence of the field and setting it equal to the density of electric charges, we take the four-divergence of our force per unit mass [per unit volume], getting:

$$\nabla^2\phi - (1/\rho_o c^2)(\partial^2 E_o/\partial t^2) + (1/\rho_o c^2)^2(\partial E_o/\partial t)^2 = 4\pi G\rho_o, \quad (1)$$

where c is the vacuum speed of light, ρ_o and E_o are the rest matter and energy densities of the test body respectively, and G the Newtonian constant of gravitation. As it stands, this expression does not have the form of customary field equations where the temporal and spatial variation of some appropriate field quantity is set equal to the local density of sources of the field. To recover such an equation we invoke Mach's principle which, in its strong form, asserts that the masses of objects are a consequence of nothing more than their gravitational potential energies – where one takes into account the potential produced by all of the matter in the universe. That is,

$$E = m\phi, \tag{2}$$

where ϕ is the total gravitational potential. As shown many years ago by Sciama (1953), the gravitational induction of inertial reaction forces requires that the locally measured value of ϕ must be equal to the square of the vacuum speed of light, so asserting that $E = m\phi$ is the same as asserting that $E = mc^2$. Using this relationship between energy, mass, and gravitational potential we are able to reduce the above expression for the inertial reaction force field to:

$$\nabla^2\phi - (1/c^2)(\partial^2\phi/\partial t^2) = 4\pi G\rho_o + (\phi/\rho_o c^2)(\partial^2\rho_o/\partial t^2) - (\phi/\rho_o c^2)^2(\partial\rho_o/\partial t)^2 - c^{-4}(\partial\phi/\partial t)^2 \tag{3}$$

Now we have a classical wave equation, the d'Alembertian of the potential of the field, set equal to its local sources. That is, a standard, relativistically invariant field equation. Note that this equation has several terms on the RHS that depend on the rate of change of the local matter (or equivalently energy) density as local sources of the field. So when test bodies are accelerated by external forces, their masses deviate from their normal values during the acceleration as their energies change.

The two terms in this equation that are of particular importance for rapid spacetime transport are those that involve the first and second time derivatives of the local matter (or energy) density, for that is something that can be manipulated with suitable apparatus. Of particular importance for the most extreme spacetime transport schemes – traversable wormholes – the term involving the square of the first time derivative of the matter (and thus energy) density is especially important. *It is always negative*, and thus holds out the promise of being a source of the "exotic" matter required to make these schemes work (Woodward, 1997). We refer to it as the "wormhole" term in the equation. Recently, R. Crowley and S. Goode pointed out to us that this term is likely to be as large as the term involving the second time derivative of the energy density, something we had hitherto thought unlikely. (This may be shown by taking $\rho_o = \rho \sin\theta$ as an *ansatz* and computing the transient terms. This does not lead to an exact, self-consistent solution of the equation. But it does show that the wormhole term is the only one that displays transient behavior in this simplest approximate solution.) Indeed, we present evidence that this is true here below.

The other term in this equation that is of interest – the one involving the second time derivative of the mass-energy density – can be both positive and negative. It lends itself to the propellantless propulsion techniques described in the next section, so we designate it the "impulse engine" term.

2. The Production of Stationary Forces:

Should it actually be possible to make the mass of some object fluctuate by applying a periodic external force to it, as Mach's principle seems to allow, even if the fluctuation is quite small, it should be possible to extract a stationary force (Woodward, 1992), thereby opening the possibility of propellantless propulsion. To visualize how this works, imagine a child on a skateboard with a paddle-ball whose mass can be made to fluctuate periodically. The child hits the ball when it is slightly more massive than normal, and the elastic cord returns the ball to him when the ball is slightly less massive than normal.

(See Figure 1.) Since the inertial reaction force experienced by the child is slightly greater when he hits the ball than when the cord returns it to him, he will experience a net stationary force. To put this in semi-quantitative terms, if a periodic mass fluctuation (in an object of mass m) that goes as $\delta m = \delta m_o \sin\omega t$ is acted upon by an external force that produces an acceleration $a = a_o \sin(\omega t + \vartheta)$, then the convolution of these effects will generate a reaction force F (in addition to that expected without the mass fluctuation present) that acts on the agent exerting the external force that behaves as:

$$F = a\delta m, \tag{4}$$

which, when time-averaged, yields:

$$F = a_o \delta m_o \cos\vartheta. \tag{5}$$

However improbable this scheme may appear, it can actually be tested by experiment. The paddle-ball is replaced by a stack of piezoelectric ceramic (PZT) disks, and the child is emulated by a massive disk of brass to which the stack of PZT disks are affixed. (See Figure 2.) To drive the mass fluctuation in the PZT crystals we merely apply an alternating voltage to the stack at some appropriate frequency. This causes a power fluctuation at twice the voltage frequency (because the power is the product of the instantaneous voltage and current, and the product of two sinusoidal functions of the same frequency is another at twice that frequency), and according to Mach's principle a mass fluctuation in the stack should ensue. To recover the stationary force we seek, we need only apply a second voltage signal to the stack at the power frequency of the first signal. If we tune the mechanical resonance properties of the stack so that the first mechanical harmonic of the stack occurs at this second voltage frequency, the second voltage signal will make the end of the stack opposite the brass disk undergo a bulk oscillation at this frequency. Since the mass of the stack is also fluctuating at this frequency because of the action of the low frequency signal, when the phase of the two signals is suitably adjusted a stationary force on the brass disk should result.

Surely, you may think, this must be too good to be true. Some process must operate to prohibit propellantless propulsion. Indeed, just such a process *seems* to operate for the following reason. Consider the idealization of the PZT disks and brass reaction mass system displayed in Figure 3A. An element in which a mass fluctuation is driven is coupled to a reaction mass by a massless actuator that produces the excursion needed to extract the putative stationary reaction force on the reaction mass. If we choose our frame of reference so that the reaction mass is at rest (at least momentarily), then it would seem that in computing the force exerted by the actuator on the fluctuating mass we must take into account the fact that Newton's second law has a $v(dm/dt)$ term as well as the usual ma term. In fact, the stationary force recovered from the ma part of Newton's second law turns out to be exactly cancelled by the $v(dm/dt)$ term in this frame of reference.

Those who work with systems with rapidly changing masses know that $v(dm/dt)$ "forces" must be treated with caution. The reason is simple. They depend on the motion (the relative v) of observers, and can be made to vanish by a suitable choice of inertial frame of reference. This cannot be done with ma forces because, for non-relativistic velocities at least, masses and accelerations are separately invariant under changes of inertial frame of reference. You can't make them go away by a choice of how they are viewed (except, of course, in an appropriate accelerating frame of reference). In this case, one need only choose the instantaneous rest frame of the fluctuating mass to recover an uncancelled stationary (time independent) force. (See Figure 3B.) Since the reaction mass, which has non-vanishing v in this frame, undergoes no mass fluctuation (at the oscillation frequency anyway), no $v(dm/dt)$ term is present to cancel the ma term that is present. Such a force present in this frame must also be present, uncancelled, in all other inertial frames of reference.

A colleague has brought to our attention that Halliday and Resnick [Christman, 1997, p. 133] make essentially the same point in a problem set by asking if a train car rolling along a smooth, straight, level track will accelerate as sand is allowed to pour through a hole in the floor of the car. The answer, of course, is of course not. And since no force acts on the car as a result of the sand pouring through the hole, no force arising from the pouring sand will act on any local external agent (an engine or rocket motor) trying to accelerate the car. But momentum transfer does take place in this system, for momentum is carried by the sand. The momentum is transferred to the earth when the sand eventually hits it. The earth, however, being effectively infinitely massive, is only imperceptibly accelerated by the landing sand.

This example is instructive for the analysis of systems involving Machian mass fluctuations. The Machian mass fluctuations presumably arise because of the gravitational coupling of the accelerated object with chiefly the most distant matter in the cosmos (that, like the earth in the train car case, is effectively infinite in amount). From the train car example, it is evident that in the Machian mass fluctuation process the $v(dm/dt)$ force seen by moving observers arises from the momentum transfer taking place between the object and cosmic matter, and this force acts on the cosmic matter, not any local agent acting on the object. This has consequences for considerations of local momentum (and energy) conservation. If one considers the train car and any local agent acting on it without taking into consideration the momentum flux being carried away by the sand, local momentum conservation will appear to be violated. Similarly, if the momentum flux in the gravitational field coupling local objects to distant matter is ignored, local momentum conservation will appear to be violated.

3. The Detection of Stationary Forces:

Allowing that there is sufficient reason to go looking for the forces expected on the basis of Machian mass fluctuations rectified, if you will, by the application of a suitable periodic force, two questions arise. First, how large are such forces? And second, how should they be detected? The answer to the first question is that if the formalism presented here is naively applied to, say, a capacitor that is periodically charged and discharged by the application of a sinusoidal voltage and it is set into motion by a garden variety piezoelectric actuator, quite large forces should be easily achieved. (For a recent discussion of this point, see Mahood, 1999.) The fact of the matter is that in real experiments of this sort no such large forces are actually seen. Naive application of the above formalism, however, is inappropriate for at least two reasons. First, when one polarizes a dielectric, much of the energy delivered by the polarizing electric field goes into the creation of lattice stresses in the material, not into the acceleration of the constituents *per se*. This means that only the kinetic part of the energy stored by the applied field will produce an effect, for the potential part of the energy does not result in the accelerations required to produce the effect. This will reduce the size of any effect in real circumstances quite sharply.

The second reason to expect a much smaller effect than naive application of the formalism suggests should be present is a consequence of the fact that in polarizing a dielectric, the ions of opposite charge move in opposite directions. For example, in titanate materials (PZT being a special case of this class), desirable because of their very high dielectric constants, the ions are displaced by a polarizing field as shown in Figure 4. Now, the physical basis of the effect can be visualized by looking at the effect of a transient acceleration of a test body on the gravitational field that couples it to the distant matter in the cosmos. As displayed in Figures 5A and 5B, before and after views of the field lines, the acceleration introduces a propagating kink (radiation) in the field (similar to the case of an accelerated electric charge). Considering one of the ions in the lattice shown in Figure 4, it is evident that the kink produced by its motion will be at least partially cancelled by the kinks of some of its neighbors because they are moving in the opposite direction, again reducing the magnitude of any effect associated with the acceleration induced radiation. So, if an effect is actually present in any real system, it may be many orders of magnitude smaller that a naive calculation indicates should be the case.

All of this means that when one goes looking for this effect, the most sensitive possible means should be employed to detect it. After all, should it turn out to be real and large, less sensitive methods can always be easily implemented. The modern arsenal of very sensitive force detectors is large, encompassing myriad devices based on strain gauges, LVDTs, Hall effect devices, and so forth. They all, nonetheless, being delicate electronic devices, can be criticized on various grounds as inappropriate in the sort of environments expected in experiments designed to test for this effect, as large voltages and currents, and strong, high frequency (ultrasonic) mechanical vibrations will be present (as several referees have pointed out to us). The preferred method of detection, in light of these concerns, is that of Cavendish and Coulomb: a very sensitive torsion pendulum (see Figure 6). Torsion pendula are not without problems of their own, but they have the great advantage that force detection does not require the presence of any sensitive electronic equipment in proximity to the devices in which the force is produced. This is especially important because of the power feeds needed to activate the devices.

Once a torsion pendulum has been selected for force detection, other requirements must be satisfied. Most important of these is the manner in which power is to be delivered to the devices (shown in Figure 2) mounted on the ends of the beam suspended by the torsion fiber (see Figure 7). One may either use a multiple filament suspension, using half of the filaments for each of the two electrical paths required in the power circuit, or one may use a single filament suspension supplemented by a second electrical path connect below the beam. We have employed both techniques. The multiple filament path was earlier followed by one of us (JFW, 2000, reported in the published conference paper). The single filament approach was used by the other (TM, 1999) in his thesis work modeled, in part, on earlier work of this sort by Talley (1991, who, by the way, unexpectedly and unintentionally detected transient forces of the sort sought by us). In the work reported here, the multiple filament suspension was that chiefly used because it enabled the connection of accelerometers built into the PZT stacks (so that the mechanical behavior of the devices could be monitored in real time), and problems associated with the lower connection in the single filament system could be obviated (see Mahood, 1999 for a description of these problems).

The use of a torsion pendulum for force detection also makes mandatory the implementation of a good vacuum system. Air currents produce motions far larger than those sought. Moreover, ionization of the air (corona) and "sonic wind" effects can completely swamp very small forces, even in moderately good vacua (*i.e.*, on the order of a Torr). These problems can only be solved by operating the pendulum in a vacuum of, at a maximum, several tenths of a Torr. And in practice one finds that a vacuum of less than 50 microns (0.050 Torr) is best. The other equipment needed to do this sort of experiment is fairly straight-forward: signal generation, mixing, and amplification equipment; a fairly broad band stepup transformer to deliver power signals with amplitudes of up to a few hundred volts; a laser and sensitive beam location detector to monitor the laser beam reflected off of a mirror affixed to the suspended assembly; a data acquisition system; sundry electronic gear (for example, oscilloscopes) to monitor and manipulate the apparatus; and a damper to bring the torsion beam to rest in some reasonable amount of time. We deal with some details related to these matters in the next section.

4. Recent Hardware and Instrumentation:

The experimental results reported below were obtained with a system that integrated the best elements of the two systems just mentioned and was substantially upgraded in several respects. We summarize here the chief improvements. First, the second generation vacuum system built initially by TM (for thesis work) was modified by the addition of a column that could be raised and lowered with a screw drive remotely, the addition of an optical quality port (to eliminate fluctuating distortions of the laser beam as it moved), and very careful, aggressive resealing. All parts of this system save the torsion head and fiber housing are shown in Figure 8. Where the best vacuum attainable prior to these modifications was about 130 microns, afterwards vacua in the 2 to 10 micron range were routinely obtained (albeit with a larger vacuum pump). Almost all of the data taken were obtained with vacua of less than 5 microns – two orders of magnitude down from the regime where corona and sonic wind complicated matters. Second, although

operability in the single filament mode was preserved, the multiple filament suspension was that chiefly used for the reasons already mentioned. Third, a new torsion beam, shown in Figure 7, was fabricated. It was designed to maximize the isolation of the beam and suspension from the vibration produced in the devices when activated (see Figure 9). And it was also configured so that the horizontal orientation of the devices could be easily changed without disturbing other parts of the system. This was done so that a test described below could be carried out. A 145 gram brass cylinder was suspended by a rod from the beam to keep the system vertically aligned (a suspension tensioning mass) and also to suppress any vibration in the damper – a plastic disk into which a several thin brass rods of varying length were glued. The brass rods were immersed in vacuum pump oil contained in a plastic cup that was raised and lowered on the aforementioned column (see Figure 10). Fourth, steps were taken to further isolate the vacuum chamber and its contents from building vibration (several components of which are visible in Figure 8).

A data acquisition system used in earlier work was adapted (chiefly through software modifications) for use with this apparatus. This eliminated the possibility of observer bias creeping into the detection and recording of data. Equally important, we found that the behavior of the devices tested was very sensitive to operating conditions, especially their temperature. To ensure consistent, repeatable behavior thermal stability had to be achieved. This meant, in practice, that the power pulse delivered to the devices had to be precisely the same length each time, and the power pulses had to be delivered at exactly the same intervals. The power pulse duration used at the outset was 3.5 seconds. With the slow degradation of the system over several weeks, the power pulse duration was later increased to 4.0 seconds. In all but special circumstances a cycle delay interval of 5 minutes was employed. This allowed sufficient time, with light damping, for the torsion beam to come to rest. At the power level routinely used, about 100 watts total into the two devices, this led to operation at about 15 degrees Celsius above the ambient temperature of the lab (recorded with spiral bimetalic strip thermometers attached to the brass reaction masses, (see Figure 11). Deviation from the equal delay interval timing of the cycles by even a minute could produce detectable variations in the patterns of the data that would persist through several subsequent cycles.

In early work the motion of the pendulum beam was detected by visually recording the motion and location of the dot produced by the reflected laser beam on a scale located about 3 meters from the suspension. Even with video recording for later visual analysis, owing to diffraction and interference effects in, and distortion of the beam, the location of the dot on the scale could not be reliably gauged to better than about a half millimeter. And with visual recording of locations the possibility of bias (*i.e.*, wishful thinking) was ever present. To improve the accuracy of the beam dot location determination and eliminate contamination by wishful thinking, an electronic beam dot location detector was built around a gradient density filter and a solar cell. With careful design, construction, filtering, exclusion of stray light, and preamplification, this system made it possible to determine differential beam dot locations to a precision of 0.01 mm, notwithstanding that the dot was visually diffused over several mm. The detector was mounted on a screw driven slider that made horizontal positioning easy, and allowed *in situ* calibration to be done by moving the detector past the stationary beam in known increments with the screw drive. This assembly is shown in Figure 12. (Such calibrations were routinely done two or three times a day, and whenever there was any reason to suspect that anything that affected this measurement had changed.) This calibration protocol permitted beam dot locations to be determined to an accuracy approaching the precision of the measurements, that is, a few hundredths of a mm.

From the outset, this apparatus has been provided with sense resistors in the high voltage circuit that activates the PZT stacks so that the instantaneous voltage and current, and their product – the instantaneous power delivered to the devices – could be monitored. With rectification and filtering, the average power applied to the devices could be (and was) recorded. Recent upgrades also made possible the recording of two other parameters of interest in this system. The first and second time derivative terms in Equation (3) lead to mass fluctuations that go as:

$$(\phi/\rho_o c^2)(\partial^2\rho_o/\partial t^2) \quad \rightarrow \quad \partial P/\partial t, \tag{6A}$$

$$(\phi/\rho_o c^2)^2(\partial\rho_o/\partial t)^2 \quad \rightarrow \quad P^2, \tag{6B}$$

where P is the power being applied to the PZT stacks (as $\rho_o = E_o/c^2$ and P is proportional to dE_o/dt). Since the real time instantaneous acceleration of the stacks is measured by the accelerometers embedded in them, if $\partial P/\partial t$ and P^2 are computed electronically in real time, they can be multiplied by the accelerometer signal, a that is, and integrated electronically to give time-averaged values that should track the effects that are predicted to be present in the system. Multiplier, differentiator, and integrator circuits were built to carry out these functions, though the P^2a circuit that tracks wormhole term behavior was only brought into operation toward the end of the period of data gathering. These circuits make possible comparison of prediction with observation without introducing the uncertainties inevitable in any purely theoretical calculation of expected behavior owing to ignorance of the detailed behavior of the system. But since the accelerometer signal is dominated by the response at the first mechanical harmonic of the PZT stacks, the P^2a circuit response does not exclusively track the response at the fourth harmonic of the low frequency applied voltage signal. Additional circuitry, not yet built, is required to suppress the lower frequency signal at the first mechanical harmonic to bring out the behavior predicted at this frequency. A block diagram of the circuits mentioned here is to be found in Figure 13.

5. Experimental Protocol:

The data collection protocol followed in this work consisted of the following steps:

1. Set the relative phase of the signals produced by the low and high frequency voltage waveforms. This was done by displaying the unmixed waveforms on an oscilloscope and moving the higher frequency waveform relative to the low frequency waveform by the manual adjustment of a phase shifter built into the signal generation circuitry (see Figure 14).
2. Start recording data [at exactly 5 minute intervals in almost all cases] four seconds before the mixed signal is applied to the PZT stacks [automatically switched by one of the DAC channels of the data acquisition system].
3. Deliver the automatically switched power pulse [with a duration of either 3.5 or 4.0 seconds].
4. Continue recording data for several swings of the pendulum [with a 16 second period]. Data is acquired at a rate of 50 Hz. The first 25 seconds of each cycle was stored as a separate file at this time resolution. And the full 80 second acquisition interval was average to a rate of 10 Hz. and scanned for the peaks of the swings, those being recorded (along with the power and integrator information) into an array in which data for multiple cycles was stored.
5. Repeat for the next phase setting.

Except for special tests, one of two phase sequencing protocols was followed. In both cases shifting back and forth between phase settings 180 degrees apart was used because a switch facilitated simple phase inversion. Since the power in the pulses varied with phase, but was about the same for phases 180 degrees apart, this switching back and forth had the desirable result that thermal effects due to changing power with phase could be largely eliminated. In the early part of data acquisition the sequencing X, X+180, X+180, X degrees was used, the next sequence then starting with X+45 degrees. In later work the sequencing X, X+180, X+45, X+225, . . . was employed. For the special tests where one of these two sequencing protocols were not used, no phase variation was done (for reasons explained below).

The amplitudes of the generated low and high frequency signals, except in a few special circumstances, were left unchanged through out the process of data acquisition. The use of fixed waveforms was adopted to insure that comparisons of the data from different runs were based on comparable data. One of the exceptions was when the devices were driven with a pure sine wave at the lower frequency. In this case the power level was varied in order to determine the response to simple changes in the power level. This was part of a particularly important test that is described below.

6. Data Recovered:

For each power pulse cycle the following data were automatically recorded:

1. The zero point and maximum peak-to-peak excursion of the laser beam dot on the photo-detector [in ADC counts for later conversion with a calibration data sequence to millimeters]. Several subsequent extrema of the laser dot position were also recorded so that the possible displacement of the zero point during the swings and any decay thereof could be evaluated.
2. The average power delivered to the PZT stacks during the power pulse interval.
3. The integrated value of the predicted force, that is, the impulse delivered by the power pulse [the integration of the product of a from the accelerometer(s) and the differentiation of the power P].
4. The integrated value of P^2a [for later runs].
5. A file with the raw data recorded at a 50 Hz. rate for the first 25 seconds of the cycle.

In addition to this, the relative phase of the high and low frequency voltage signals and the value of the vacuum in the chamber were manually added to each of the automatically recorded cycle data files. The formal data presented here were obtained between 31 December 1999 and 19 January 2000.

7. Results:

The first series of runs with the apparatus described above were done between 31 December 1999 and 5 January 2000 using the X, X+180, X+180, X, X+45, . . . protocol for the variation of the phase. Because the stepup transformer sharply attenuated the high frequency component of the amplified mixed waveform, almost all of the power delivered to the test units (more than 90% for all phases) was at the lower frequency. To illustrate this behavior, as an example we show the mixed waveform for 0 degrees of phase and the resulting actual voltage waveform in Figure15. The data obtained, averaged by day and type of run, for the measured maximum excursion versus relative phase are displayed in Figure 16. Two things are immediately apparent in these data. First, the maximum excursion depends on the phase, with a periodicity of 360 degrees. **Note that 360 degrees of phase here (and elsewhere in the following) refers to the higher frequency of the applied voltage signals (and the power frequency of the lower frequency signal) – that is, a "two omega" signal, "omega" being the frequency of the lower frequency signal.** Second, the displacement of the individual curves from each other, in the case of the daily averages, reveal slow decay of the response of the system. Nonetheless, the variation of the maximum excursion with phase is largely unaffected by this systematic long-term decay in the total amplitude of the excursions. Eventually, this behavior was traced to a radiometer effect arising from the residual air in the vacuum chamber interacting with the test units whose temperatures were raised during the application of the power pulses. The aluminum caps heated more rapidly than the brass disks, leading to gas scattering from the aluminum caps acquiring more recoil momentum, and thus a net force on the test units for the several minutes that this temperature imbalance persisted. The early data were taken with a chamber pressure of 5 to 7 microns, and the late data (after continuous pumping) were acquired with a chamber pressure of 2 to 2.5 microns. Because this radiometer effect has a slow onset and long decay constant, however, it does not produce an excursion of the beam that masks the swing produced by the prompt Machian effect, which starts immediately and ceases with the removal of the power pulse. To show that the variation of maximum excursion with phase is largely insensitive to the systematic decay of this radiometer effect, we adjust the data for each set of averages by a constant additive "normalization" so that they overlie each other. This is shown in Figure 17. And the data so arranged can be used to generate the curve in Figure 18, where the error bars are the standard deviations of the adjusted values of all the curves for each phase. Evidently, the variation of maximum excursion with phase is not a statistical fluke.

Perhaps the first thing that should be said about Figures 16 through 18 is that the beam moves when power is applied to the test units notwithstanding that great care was taken to eliminate all causes of

motion other than the effect sought. You may not think this too remarkable, for the force that corresponds to the induced motion is less than a dyne, a very small quantity, and absent demonstration otherwise it is easy to believe that such a small force may be caused by some spurious mechanism. And evidence of a thermal pulse induced radiometer effect is apparent. We address this issue in the next section. The second noteworthy feature of the maximum excursion versus phase displays is that a clear "two omega" periodicity is present. This is the signature of the "impulse engine" term in Equation (3) above. The presence of this periodicity in the data is more impressive yet when one examines the integrated force (impulse) measurements that should correlate to this maximum excursion periodicity if it really arises from an impulse engine effect. The integrated force versus phase data that corresponds to this maximum excursion data is presented in Figure 19. Like the maximum excursion data, it too displays the two omega periodicity characteristic of the impulse engine term. More importantly, it has the correct phase relationship to the maximum excursion data. (No attempt was made to absolutely calibrate the PZT stack accelerometers, so no quantitative prediction is made here. Absolute calibration was not done since there is no reason to expect such a quantitative prediction to correspond to the actual impulse for the reasons set forth earlier.)

If we provisionally accept the two omega periodicities in the maximum excursion and impulse data in Figures 16 through 19 as evidence that the predicted mass fluctuations and stationary forces in devices of this sort may really be present (albeit at a level far below that suggested by naï ve calculations), we may ask: Where is the predicted four omega behavior that should be present because of the wormhole term in Equation (3). Since the variation with phase in Figures 16 to 19 is not exactly sinusoidal – as would be expected were only an impulse engine effect present – one might argue that evidence for higher harmonics is already apparent. This, however, understates the actual circumstances, as becomes evident when one examines the averaged power data that corresponds to the data in Figures 16 to 19. The averaged power data is shown in Figure 20. We note immediately that the power varies by about 15% as the phase changes (notwithstanding that the amplitudes of the low and high frequency waveforms that are mixed to produce the voltage signal are held constant). Moreover, the periodicity of the power changes with phase is four omega – the periodicity expected of wormhole term behavior. Can it be that wormhole term behavior is actually present, but largely suppressed in the maximum excursion data because of the power changes that accompany the phase changes? Is it, to at least some extent, being cancelled by the radiometer effect which will vary with the power as the phase is changed?

The answer to this question can only be supplied by determining the behavior of the system when the power level is changed without changing anything else. This may be done by applying the low frequency sine wave alone to the system. Assuming that this waveform is pretty clean (as in fact it is), you may think that, aside from thermal effects [with long time constants], no excursion of mechanical origins should be induced because of the symmetry of the applied signal. This, however, neglects the fact that the first mechanical harmonic of the PZT stacks is the second harmonic of the applied voltage signal. This will surely be excited by the power wave of the low frequency signal. And since the PZT stacks are highly ferroelectric, they will further affect the electromechanical properties of the stacks when activated. That this is the fact of the situation is easily seen in Figure 21 where the power and $\partial P/\partial t$ waveforms in the high voltage circuit for a pure sine wave driving signal are displayed. As long as these waveforms simply scale in amplitude with the power (which in general they won't because of the nonlinearities in ferroelectric materials), we can answer our question. And we should expect non-thermal motion because of the interaction of the four omega P^2 mass fluctuation with the four omega mechanical excursion excited as a higher harmonic of the applied voltage signal. If the waveforms in Figure 21 are independent of amplitude over the power range in question – as they in fact are – then the maximum excursion should scale linearly with the power.

"Sine only" (*i.e.*, single frequency waves of the sort just discussed) power variation data taken between 31 December and 5 January that span the powers encountered in the mixed waveform data are presented in Figure 22. Like the data shown in Figure 16, they display the same secular day-to-day evolution. And, as expected, they show that the maximum excursion scales linearly with the applied power. To compare

these data with those in Figures 17 and 18, we can adjust the data for each day to an imaginary line that lies midway between the extremes. (As no sine only data were taken on 3 January, such data cannot be used as a locator for this line.) The adjusted data, together with their regression line, are shown in Figure 23. We note that at the 100 Watt power level a maximum excursion on the order of 8 mm occurs. But in the mixed waveform data in Figures 17 and 18 the maximum excursions for 45, 90, and 270 degrees, where the power levels were about 100 Watts, are all smaller than 8 mm. Evidently, something acts to suppress the excursions that would otherwise be expected given the applied powers in much of the mixed waveform data. With Figures 18 and 23, we can calculate and plot this deviation from expectation that the maximum excursion should simply scale linearly with power. This deviation is laid out in Figure 24. The error bars from Figure 18 have been adjusted to account for the uncertainty in the sine only values. Now the four omega as well as two omega behavior is obvious. It would appear that both the impulse engine and wormhole terms contribute to these results, and the wormhole contribution is larger than the impulse engine part, as predicted. But before this conclusion can be accepted, we must first investigate other potential causes of the behavior seen. It would be foolhardy to accept these results as evidence of Machian mass fluctuations if they can be accounted for in terms of other known causes.

Before turning to the checks done to identify the source of the signals identified here we address one further point. How large are the forces detected in this experiment? With the known parameters of the system, calculation of the forces detected is a fairly straight-forward matter. One can either use a simple ballistic torsion pendulum approximation (because the power pulse is a small fraction of the pendulum period) or the somewhat more elaborate techniques discussed by Mahood (1999). Both approaches yield essentially the same answer. The forces are on the order of several hundredths of a dyne in each of the test units. *These are not large forces.* So, even should they prove genuine, it is not obvious that they can be engineered to practical levels, though there are reasons to believe that this may be possible.

8. Sources of Spurious Signals:

For any spurious source of motion to pass muster it must account for forces on the beam that lead to the observed excursions of the laser dot seen with the detector. Ignoring mass fluctuations, this means that the activation of the test units must lead to a torque on the beam through coupling of the devices to the surroundings, where the surroundings are understood to include the torsion fiber and damper. In other words, somehow they must push off of something when they are activated to produce the observed rotation of the beam. View from this perspective, potential sources of spurious motion can be grouped into a few natural classes: those due to residual gas in the vacuum chamber; those that arise from electromagnetic coupling(s) to the surroundings; mechanical effects that react through the suspension fiber and/or damper on the vacuum case; and thermo-mechanical effects caused by the heating of the parts of the system during activation. We deal here with each in turn.

Residual Gas: Three effects come under this heading: “sonic wind”, coronal discharge, and radiometer effects.

- Sonic wind arises from the nonlinear interaction of residual gas with vibrating parts of the device and are especially apparent when the amplitude of the vibrations of various parts of a device are different, as is the case here. Indeed, from atmospheric pressure all the way down to a few Torr, sonic wind effects swamp all others. At a few Torr one finds that there is insufficient residual gas for this effect to operate.
- But at a few Torr, unless the high voltage parts of the devices have been carefully sealed, coronal discharge becomes quite prominent. It is easily detected in low background light levels by its distinctive violet glow. It can be essentially eliminated by careful insulation and operation at vacuum levels well below a Torr. Ultimately, to insure that coronal discharge was absent a very sensitive, broad band image intensification scope was used late at night with even displays and indicator lights blacked out to check for any discharge. None that could account for the excursions seen was found.

- Radiometer effects arise from the differential heating of parts of the test units so that reflected atoms of residual gas acquire more momentum is some locations than others. In this case, heat is evolved in the PZT stacks during the power pulses and is conducted to the brass disks and aluminum caps, as already discussed. The aluminum caps heat more rapidly than the brass disks, so radiometer effects cannot be simply set aside without careful consideration. The chief reason for excluding radiometer effects as the source of even the bulk of the signals seen is that they don't have the right signature. The effect seen is prompt. Its onset can be seen within 100 milliseconds of activation. (See Figure 25 in this connection.) And while thermal effects, including radiometer effects, can easily be seen in the data well after the power pulse is under way, it takes several seconds or longer for these effects to manifest themselves as it takes at least that long for the heat to be conducted from the interior of the PZT stacks to the other parts of the device (as revealed by the thermometers attached to the brass disks). Moreover, the forces associated with these effects do not go away when the power is shut off. They continue to act until the heat is dissipated, producing seen signatures (zero offset of the torsion beam position), but not ones that can account for the maximum excursion *variation* seen in Figures 16 through 18 as the phase is changed. In addition, radiometer effects in particular, and thermal effects generally, should scale with the power in the applied pulses. Comparison of Figures 20 and 18 shows clearly that no such correlation exists in fact in these data for the part of the excursion that undergoes the sought variation with $\partial P/\partial t$ and P^2 (see Equations 6A and B above). At any rate, no such correlation exists until after the correction explained above is applied to the data to compensate for the radiometer effect's suppression of the four omega behavior of the devices.

Electromagnetic Coupling to Surroundings: The sorts of effects envisaged here are those where the currents in and fields surrounding the test devices and their power feeds couple to materials in the surroundings and/or the Earth's magnetic field. They fall into four categories: alternating and static electric and magnetic fields either in the environment or induced by the delivery of the power pulses to the test units. Although in some cases they overlap, we deal with each of these categories sequentially.

- Alternating electric fields are not expected to be large in the vicinity of the test units, for such electric fields as are present will be essentially completely confined to the dielectric material between the plates of the PZT disks. But they will be present around the power feeds, as one of the two feeds carries a voltage that alternates between +150 volts and –150 volts. The resulting alternating electric field can drive eddy currents in nearby conductors and alternating polarization in close-by insulators. The induced polarization in insulators can interact directly with the electric fields produced by the power feeds, and any induced currents can interact magnetically with the current in the feeds. We leave magnetic effects for later consideration and focus on purely electric effects here. We note that the interactions we are contemplating here consist of the action of induced dipoles in surrounding insulators on the electric charges that create the fields that induce the dipoles. This interaction will be self-rectifying. That is, when the voltage and electric charges change sign, the induced dipoles will reverse orientation. Accordingly, notwithstanding that the electric fields and induced dipoles time-average to zero, this sort of interaction can create a force that always acts in the same direction on mobile components of the system. The obvious way to exclude such effects is to discover how large they are. This is easily done by applying a DC voltage equal to the peak alternating voltage to the system and observing the resulting behavior. When this was done a small effect was in fact seen. But it was far too small (down by more than an order of magnitude) to account for the excursions routinely produced in the apparatus. Another way to check for the presence of such effects is to place a large slab of insulator (a sheet of plastic a little more than a centimeter thick) against the vacuum chamber and look for changes in the performance of the system. This done, no changes were noted.
- Static electric fields are already eliminated by the DC voltage test used to estimate the induced dipole forces for alternating electric fields. They are not the source of the signals seen.

- Alternating (electro)magnetic fields may be expected to induce eddy currents in nearby conductors, those eddy currents in turn acting back on the currents in the feeds and test units to produce forces that might induce torques on the torsion beam. For this reason, one minimizes the presence of conductors near the feeds and test units. And such conductors that must be present are made from non-ferromagnetic materials. (Stainless steel and brass fasteners were used exclusively in the system as a result.) The simplest way to test for the presence of these effects is to place substantial sheets of conducting materials near the vacuum case to see if they have any effect on the system. The results of these tests are to be found in Figures 16 and 17 where the effects of aluminum and steel plates placed near to the vacuum chamber are displayed. Evidently, these tests do not reveal any effect of electromagnetic coupling.
- Given the fairly high frequency of the signals applied to the test units and the care that was taken to keep the conduction paths to and from the units close together, it seems unlikely that any significant interaction with static magnetic fields should take place. But the Earth's magnetic field is ever present, so this must be considered. (Static magnetic fields could have been nulled with Helmholtz coils, but given the expanse of the region where nulling would have to have been done, this option was never seriously considered.) The way to check for the effect of static magnetic fields is to intentionally apply a known field comparable to the ambient fields and observe its effect on the performance of the system. This was done with a stack of ring ferrite magnets (shown next to the optical detector in Figure 12) with a flux of 1.4 kiloGauss at the poles. At a distance of 54 cm. these magnets produced a field of about 1.6 Gauss, that is, about three times the strength of the ambient magnetic field. The magnets were placed in three orientations with respect to the system: radially (with the axis of the dipole pointing toward the test units); tangentially (with the dipole axis perpendicular to the line to the center of the system); and vertically (with the dipole axis pointing up and down). As with the aluminum and steel plate tests, the results of these tests are also to be found in Figures 16 and 17. The data for the vertical and tangential orientations of the field have been coalesced, for there was no difference between them. The radial orientation results have been left separate, for where the tangential and vertical results were a bit lower than the non-test results obtained on 3 January, the radial results were a bit higher. That is, a static magnetic field three times as strong as the ambient field did noticeably affect the behavior of the system. But the size of the effect is quite small. And more importantly, the static magnetic field did not change the amplitude of the two omega variation found in the data. Were static magnetic fields the source of the signals of interest, changes in the field strength would have to have affected the amplitude of the effect. They did not. And we may conclude that static magnetic fields do not produce the effects with the impulse engine and wormhole term signatures.

Mechanical Effects Produced by Vibration: Mechanical vibration, necessarily present in the test units when activated, cannot produce a torque on the torsion beam unless they react on the suspension and damper – just as one cannot make a swing swing without exerting forces on the suspending branch above or pushing off of the ground below. Although the torsion pendulum force detection technique was adopted chiefly for this reason, nonetheless, it is easy to believe that small torques could result from the mechanical vibrations generated in the test units, notwithstanding that with frequencies of 37 kHz and higher it is very unlikely that they would couple to a pendulum with a period of 16 seconds. Two tests were developed to rule out such effects. First, the torsion beam was designed to allow horizontal reorientation of the test units so that they could be both reversed and pointed toward each other, leading to three operating conditions: Normal, Opposed, and Reversed. Given the heavy vibration damping provided by the various rubber washers and straps (see Figure 9), such vibration as is communicated to the beam and suspension should be largely independent of the horizontal orientation of the test units. So changes in that orientation should not significantly affect any motion of the beam if simple vibration is the cause of the signals. If the effect is real, on the other hand, horizontal reorientation should reverse the direction of motion for the reversed configuration and suppress the motion in the opposed configurations. The second test involved raising and lowering the damper cup so as to change the stiffness of the lower terminus of

the suspension. If the effect arises from a reaction against the suspension, it should display behavior different from those changes expected for a real effect when the damping is increased and decreased.

- The results of the horizontal orientation variation test are presented in Figures 26 through 29. The data that are the basis of these figures were obtained at two operating frequencies, 74.0 and 74.5 kHz to see if variation of this parameter by modest amounts changed the behavior of the system. It didn't, so the data for the two frequencies have been averaged together. Figure 26 is the counterpart of Figure 16 where daily and special test data are presented without any correction for long-term secular evolution of the system. As in Figure 16, such evolution is still clearly present. But equally obvious is the fact that motion of the torsion beam is strongly suppressed when the system is run with the test units opposed. Moreover, the opposed configuration does not produce any phase dependent structure like that seen in the normal configuration, whereas the reversed configuration does, as one would expect if the signals are genuine. This is especially easy to see in Figure 27 where the data have been "normalized" in the same fashion as in Figure 17. We also note that the direction of motion does reverse in the reversed configuration, as can be seen in the representative traces for the various configurations in the first 25 seconds displayed in Figure 28. Additional evidence relating to this behavior can be gleaned from inspection of the detailed response of the system in the first few seconds of application of the power pulses. These data are presented in Figure 29. For both the normal and reversed configurations we see that the response is prompt, as in Figure 25. (Note also the fluctuation in these traces that arise from linear swing of the suspension induced by the inequality of the forces produced in the two test units.) Whereas the response in the opposed configuration is nil for nearly a second and a half – as would be expected if motion in this case arises from a thermal effect with a rather long time-constant. It is also worth remarking here that the reversal of the thermal part of the excursions evident in Figure 28 suggests that the source of the thermal part is a radiometer effect (which should reverse with orientation, unlike the other thermal effects discussed below).
- As mentioned above, the damper consisted of several brass rods glued into a plastic disk near to its periphery. In fact there were eight such rods (each $1/16^{th}$ inch in diameter). Four were a little more than a centimeter long, and the other four were six millimeters longer than the others. In order to bring the torsion beam to rest in a reasonable length of time we found it necessary to keep 3 mm of the longer rods immersed in the oil in the damper cup. In normal running circumstances the cup was raised farther still until 3 mm of the shorter rods, in addition to the 9 mm of the longer rods, was immersed. Even with this oil cup height, the cup could be raised yet farther; indeed, another 3 mm height was possible without compromising the system. This test thus consisted of delivering power pulses sequentially to the device for varying immersion depths of the damper rods. Damping could be expected to trace roughly the total length of rods immersed, that is, 12, 24, 48, and 72 mm for the four cup heights selected. Maximum excursion versus rod immersion length data are displayed in Figure 30. Simple inspection of this figure reveals that the maximum excursion decreases with increasing damping, as would be expected with a genuine effect. The maximum excursion does not increase with increasing damping as the mechanical vibration hypothesis regarding the origin of the signals seen suggests should happen. This result, together with the orientation variation test, permits one to conclude that the motion of the torsion beam seen when the test units are activated does not arise from mechanical coupling of vibrations to the suspension/damper assembly.

Thermo-Mechanical Effects: Heat is evolved in various parts of the apparatus when the test units are activated. The current in the suspension fibers and leads, for example, produce i^2R (Joule) heating. And heat is evolved in the PZT stacks too. The heat evolved in these locations during test unit activation is conducted to the other parts of the suspension/beam assembly. Fortunately, from the point of view of this experiment at least, the time constants of these thermal effects and their mechanical consequences are relatively long and so can be separated from the effects sought. This is fortunate indeed, for thermal

effects comparable in magnitude to the effects of interest are in fact present in this system and the data obtained from it. Two are particularly important: suspension relaxation and PZT stack expansion.

- Even with very careful construction and the use of annealed wire, a suspension of a dozen strands of #34 AWG copper wire will have some residual stresses. To some extent these stresses can be "burned out" by prolonged operation of the system. But some stress almost always remains. (This, by the way, is also true for single filament suspensions.) When the power pulse is delivered, Joule heating of the suspension causes this residual stress to relax, producing a torque on the torsion beam. Depending on the idiosyncratic circumstances of assembly, this effect may either impede or abet any real torque present. Unlike a real effect, where the force is switched on full-strength immediately, however, this heating effect is cumulative. So it doesn't begin to manifest itself until some time after the onset of the power pulse. Precisely this behavior can be seen in the detailed trace for the opposed configuration in Figure 29. Thermal effects in the suspension also have another signature: they cause an offset in the rest, or zero, position of the torsion beam. This is easily seen as a different midpoint for induced swings from the initial rest position. As the suspension cools, the swing mid point (and beam rest location) reverts to its previous value. The zero point offsets mentioned here can be seen in the 25 second data in Figure 28. They are typical in this regard of essentially all of the data we have obtained. The time-constant for zero point relaxation turned out to be on the order of several minutes. Because of the similarity of suspension relaxation effects to radiometer effects, they are difficult to separate from each other. But they both can be discriminated from the prompt impulsive torques produced by a real effect. They may increase, or decrease, the initial swing of the system, but because of their long decay times, they cannot cancel out the impulse delivered by a real effect, which therefore manifests itself as part of the maximum (peak-to-peak) excursion in the first full swing of the torsion beam.
- Test unit heating has several consequences. Once thermal stability is achieved, they don't produce spurious signals. But before that state is attained, strange results are easily had. The chief result of test unit heating is thermal expansion of the PZT stacks (and those things to which they convey heat). This has two effects. First, thermal lengthening of the stacks changes the balance conditions of the stacks suspended by the rubber straps beneath the torsion beam (see Figure 9). This can cause them to tilt slightly. Such tilting, however, will not produce a net torque on the beam. Second, and far more important, thermal expansion of the stack assemblies changes their conditions of preload which can drastically affect the performance of the PZT stacks. As with changing balance condition, however, these effects do not produce net torques on the torsion beam.

The above said, there is one compelling reason to reject thermo-mechanical effects as the source of the signals identified in Figures 16 through 29 as having the signature of impulse engine and wormhole term behavior. Thermo-mechanical effects scale with the applied power. As comparison of Figures 18 and 20 makes plain, the effect of interest, taken to be of mundane origins, does not correlate to the applied power.

What Does This All Mean?

Well, these devices (as well as their predecessors) certainly move when activated. And, as the check protocols just discussed reveal, their motion is the result of an internally generated force that has the distinctive signature of the Machian propulsive effect predicted by theory. Other small forces are present and identifiable too, but they do not mask the effect sought, small though it may be. As far as rapid spacetime transport is concerned, however, the operative word in the previous sentence, we note, is *small*. Were these effects orders of magnitude larger, it would be almost trivial to implement them in rapid spacetime transport schemes. So, granting the presence of a genuine effect, the problem becomes how to

make the effects larger. ***Much larger***. In this connection it is worth noting that the naï ve calculation of the size of Machian mass fluctuations leads to effects that are orders of magnitude larger than those seen in this and earlier experiments. In turn, this suggests that one examine the conditions that presumably suppress the large effects of the naï ve calculation for ways to make these effects larger. Such schemes, however, exceed the scope of this paper. But if they can be found, the sky's the limit.

Acknowledgement:

We are indebted to many who have offered advice and encouragement over the past few years. Meriting particular notice are R. Crowley, S. Goode, K. Wanser, and several unidentified referees whose comments have helped significantly.

References:

Christman, J.R., 1997, *Test Bank to accompany Fundamentals of Physics (fifth edition)* (Wiley, New York).

Mahood, T.L., 1999, "A Torsion Pendulum Investigation of Transient Machian Effects," California State University Masters Thesis, available at http://www.serve.com/mahood/thesis.pdf.

Rindler, W., 1991, *Introduction to Special Relativity* (2nd ed., Clarendon Press, Oxford).

Sciama, D., 1953, "On the Origin of Inertia," *Monthly Notices of the Royal Astronomical Society* **113**, 34-42.

Talley, R.L., 1991, "Twenty First Century Propulsion Concept," final report prepared for the: Phillips Laboratory, Air Force Systems Command, Propulsion Directorate, Edwards AFB CA.

Woodward, J.F., 1990, "A New Experimental Approach to Mach's Principle and Relativistic Gravitation," *Foundation of Physics Letters* **3**, 497-506; 1992, "A Stationary Apparent Weight Shift from a Transient Machian Mass Fluctuation," *Foundations of Physics Letters* **5**, 425-442; 1995, "Making the Universe Safe for Historians: Time Travel and the Laws of Physics," *Foundations of Physics Letters* **8**, 1-39; 1997, "Twists of Fate: Can We Make Traversable Wormholes in Spacetime?," *Foundations of Physics Letters* **10**, 153-181; 2000, "Mass Fluctuations, Stationary Forces, and Propellantless Propulsion," STAIF-2000 conference paper.

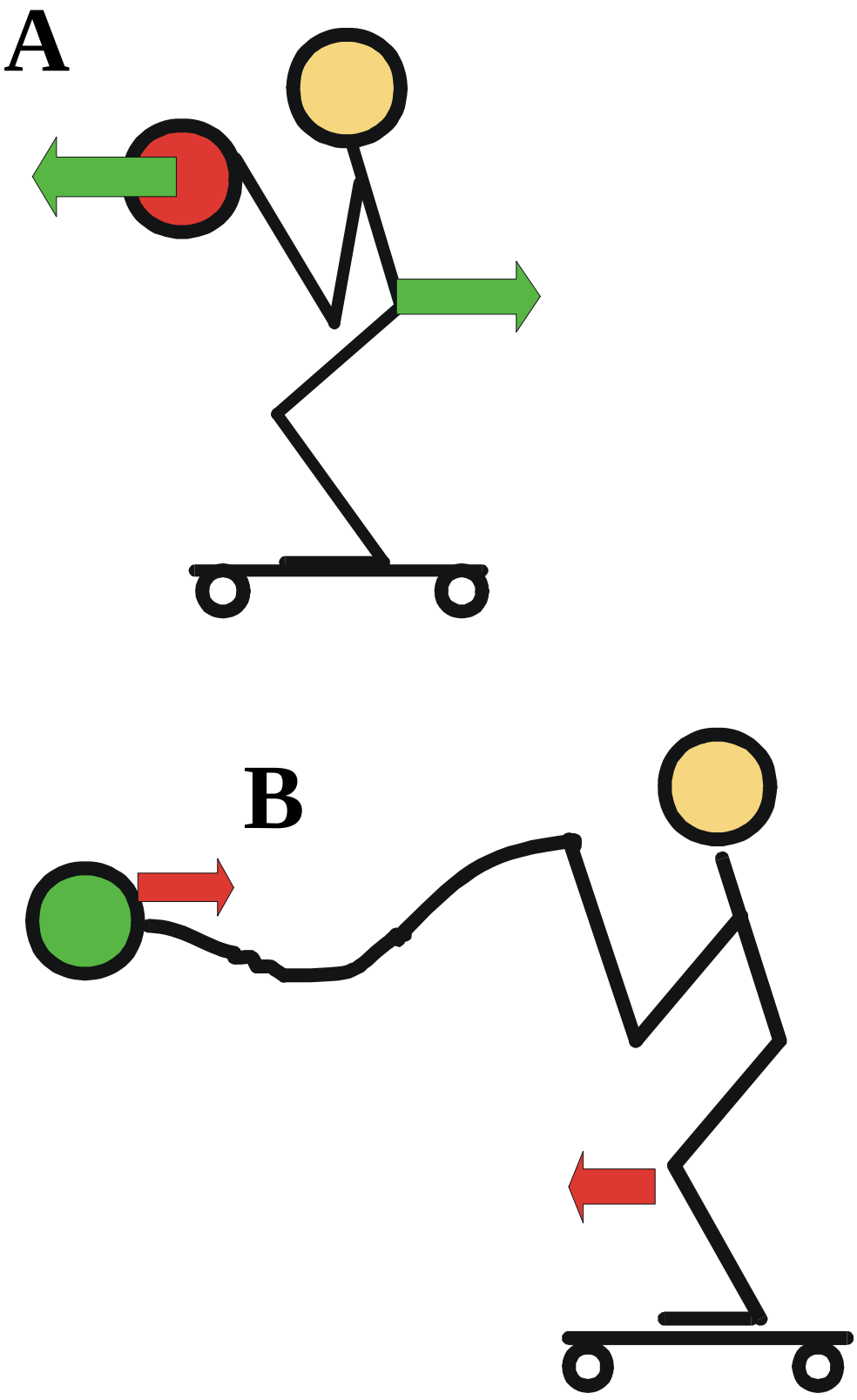

Figure 1

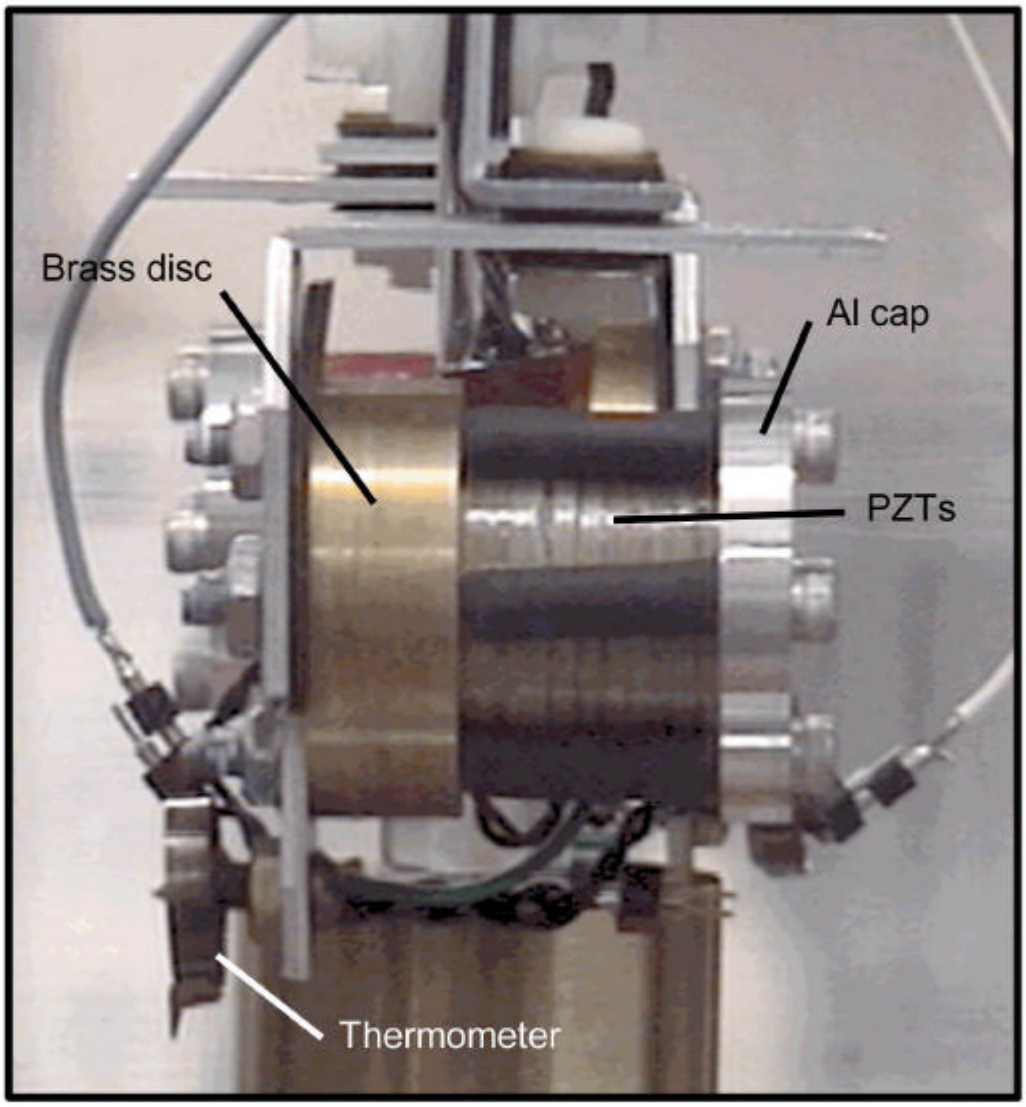

Figure 2

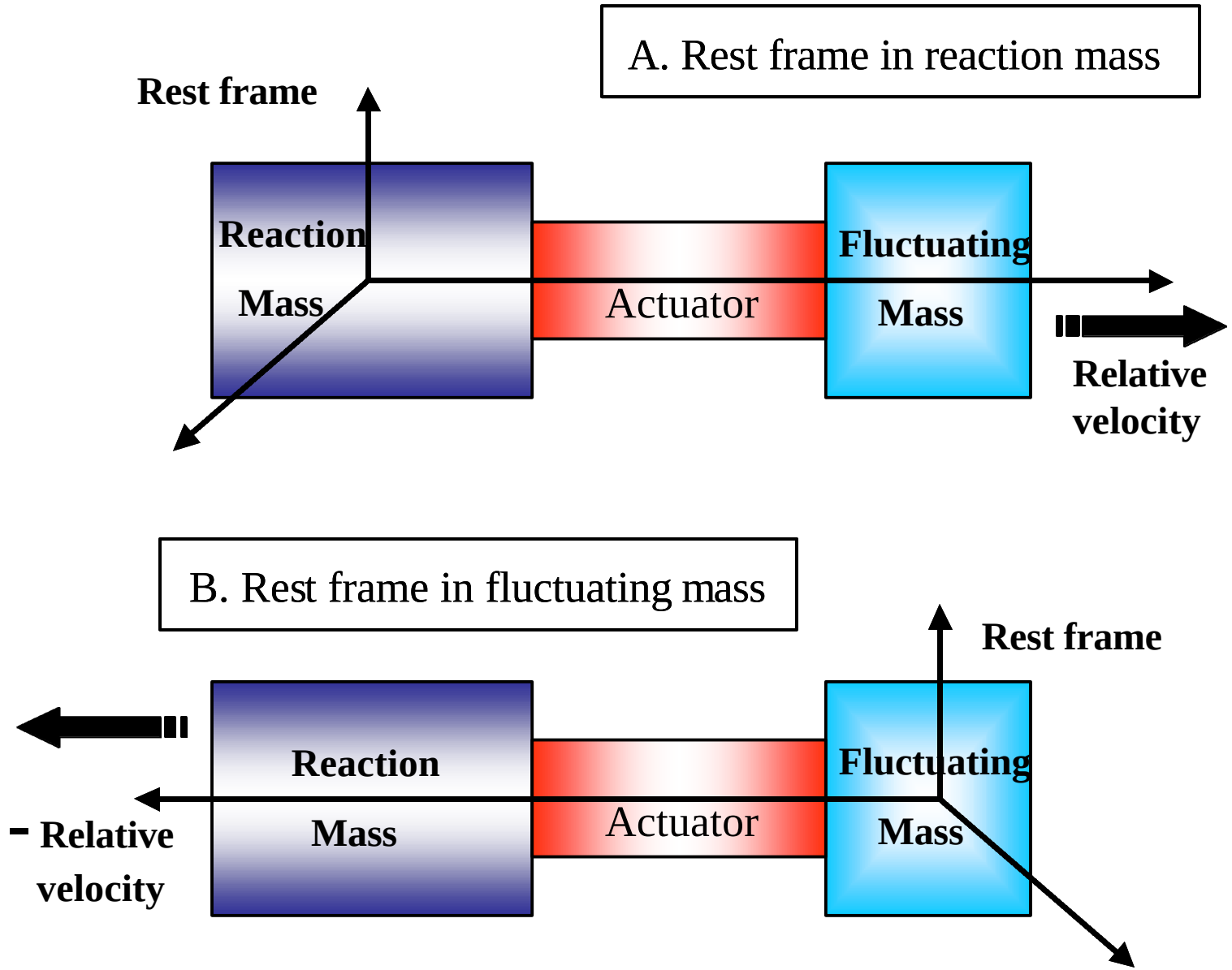
A. Rest frame in reaction mass
Rest frame
Reaction
Mass
Actuator
Fluctuating
Mass
Relative
velocity
B. Rest frame in fluctuating mass
Rest frame
Reaction
Mass
Actuator
Fluctuating
Mass
- Relative
velocity

Figure 3

Polarization response of Barium Titanate

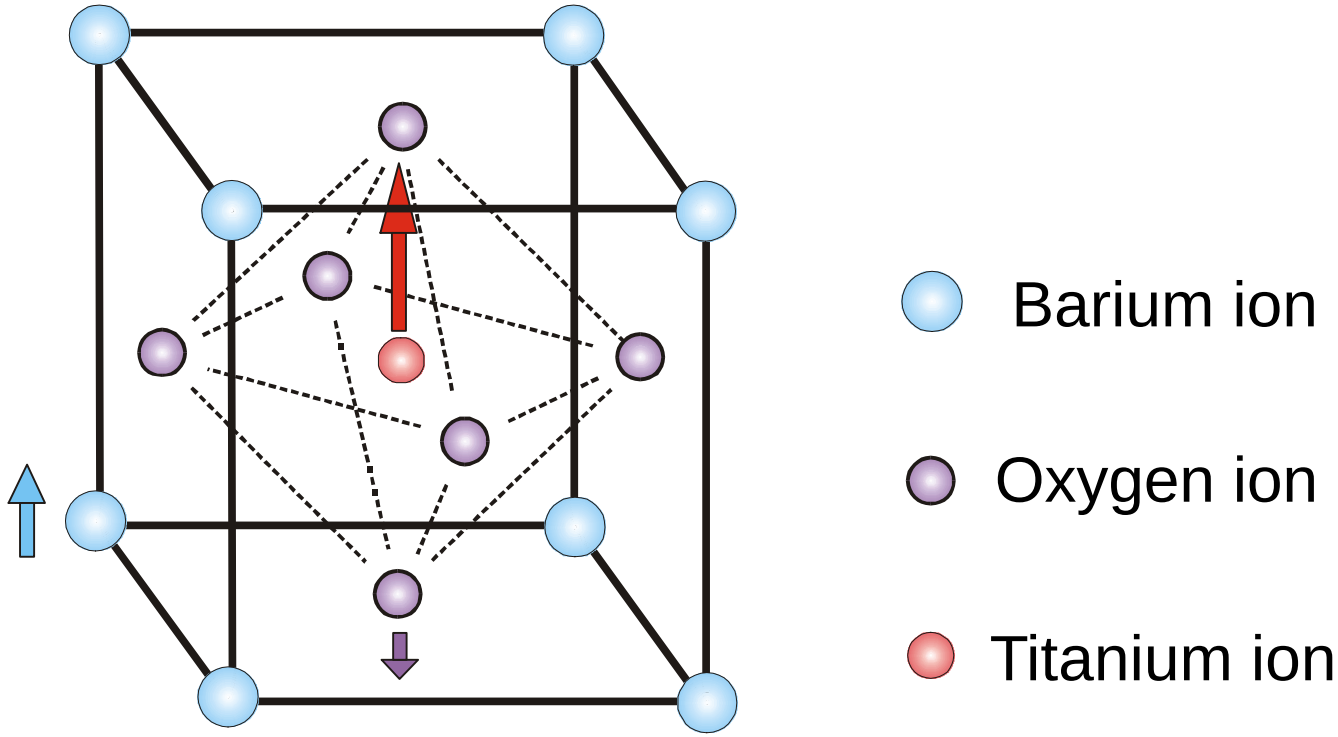

Arrows indicate direction and proportional response to electric field

Figure 4

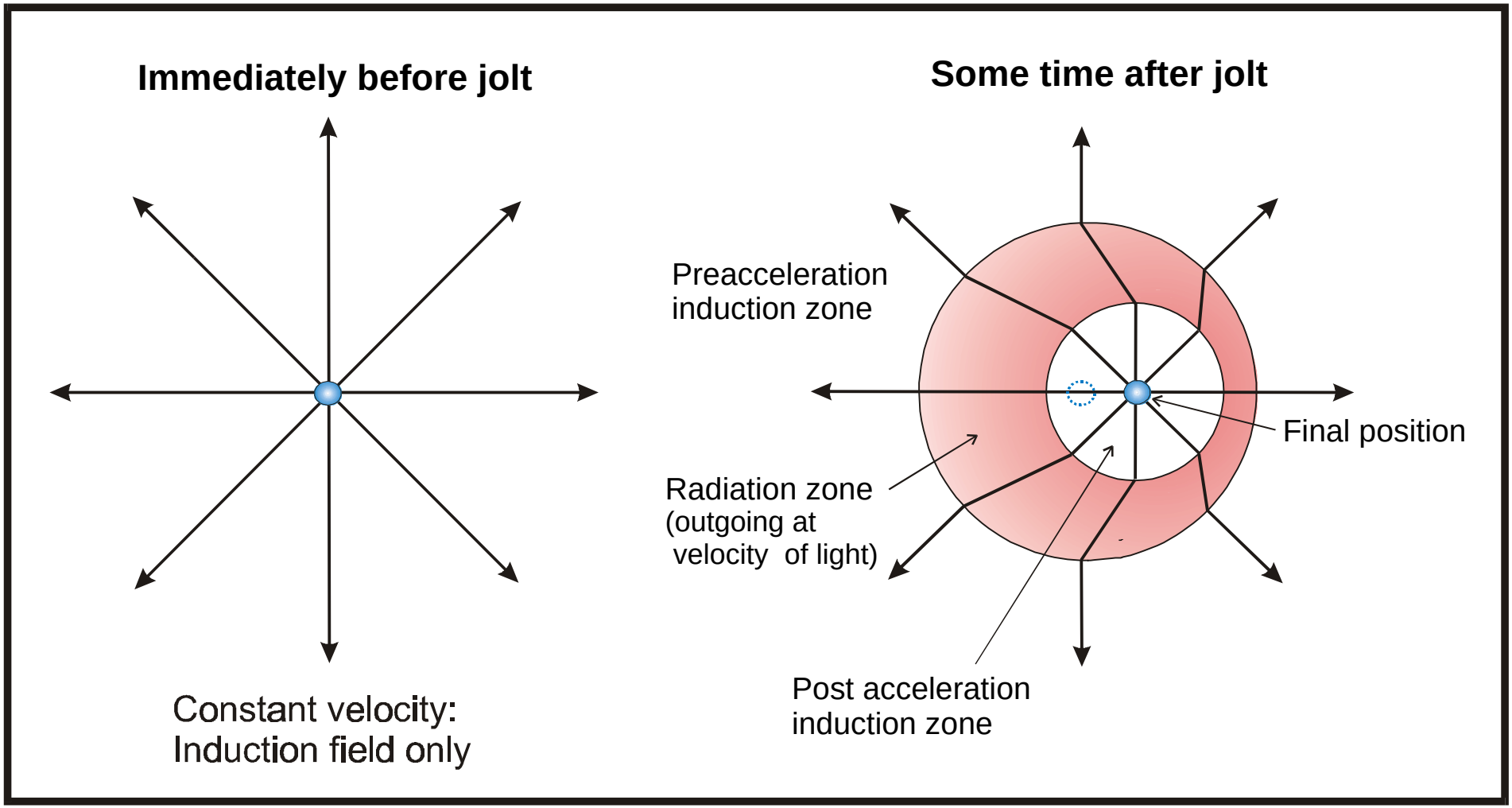
Immediately before jolt
Some time after jolt
Preacceleration
induction zone
Final position
Radiation zone
(outgoing at
velocity of light)
Post acceleration
induction zone
Constant velocity:
Induction field only

Figure 5

Torsion arm schematic

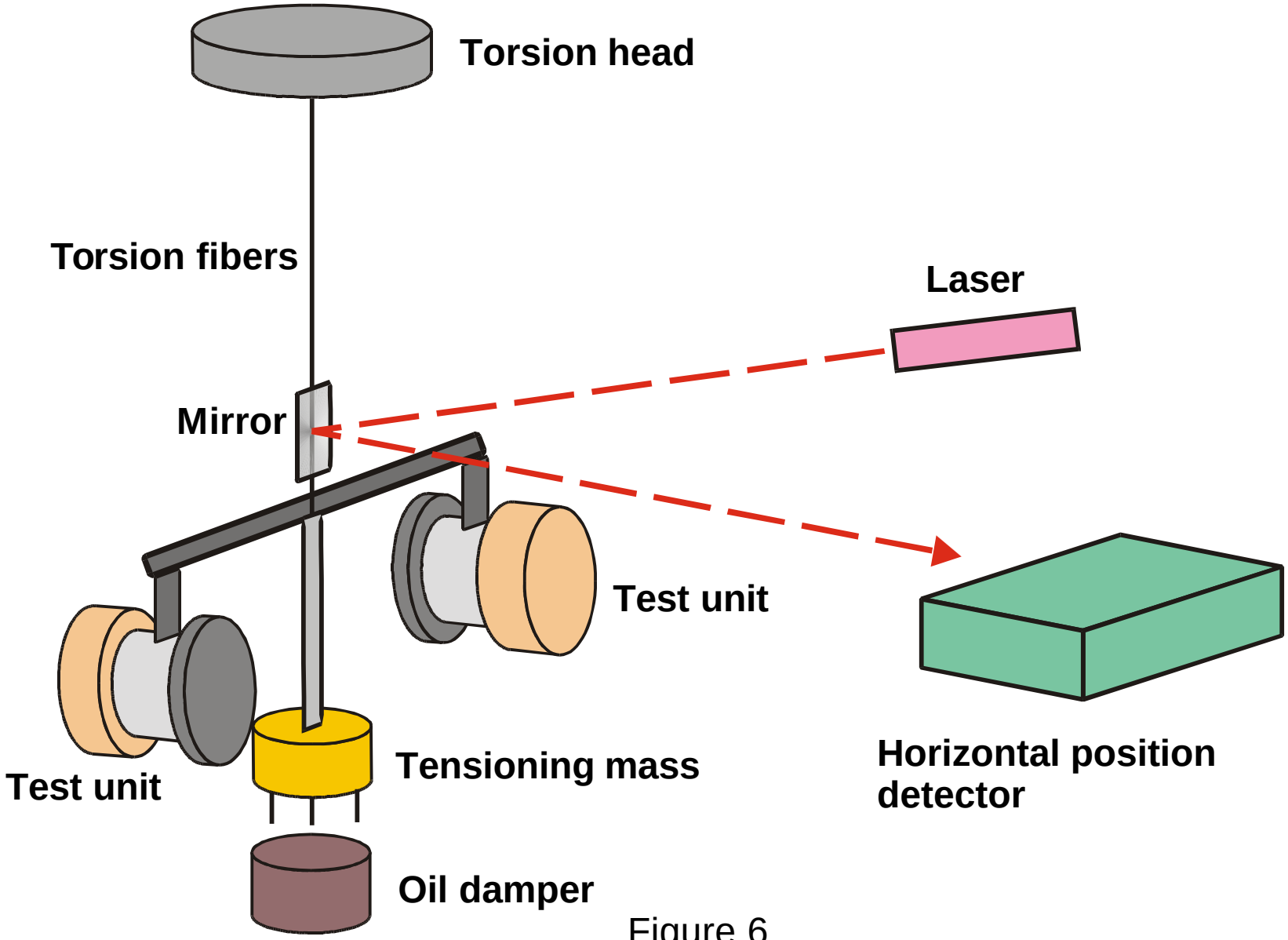

Figure 6

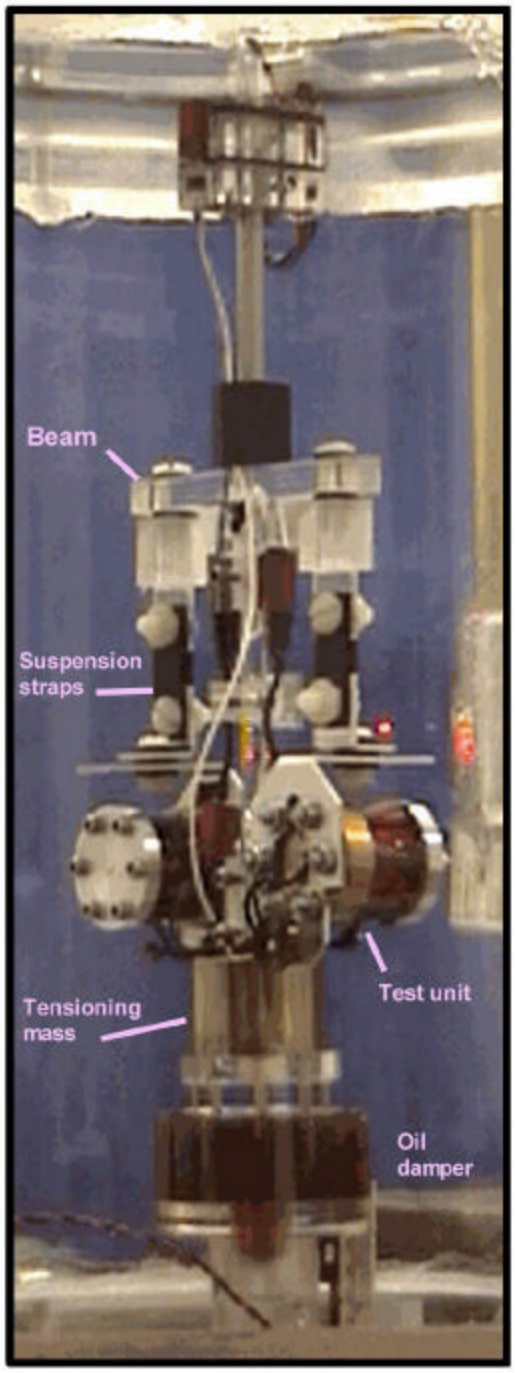
Beam
Suspension straps
Test unit
Tensioning mass
Oil damper

Figure 7

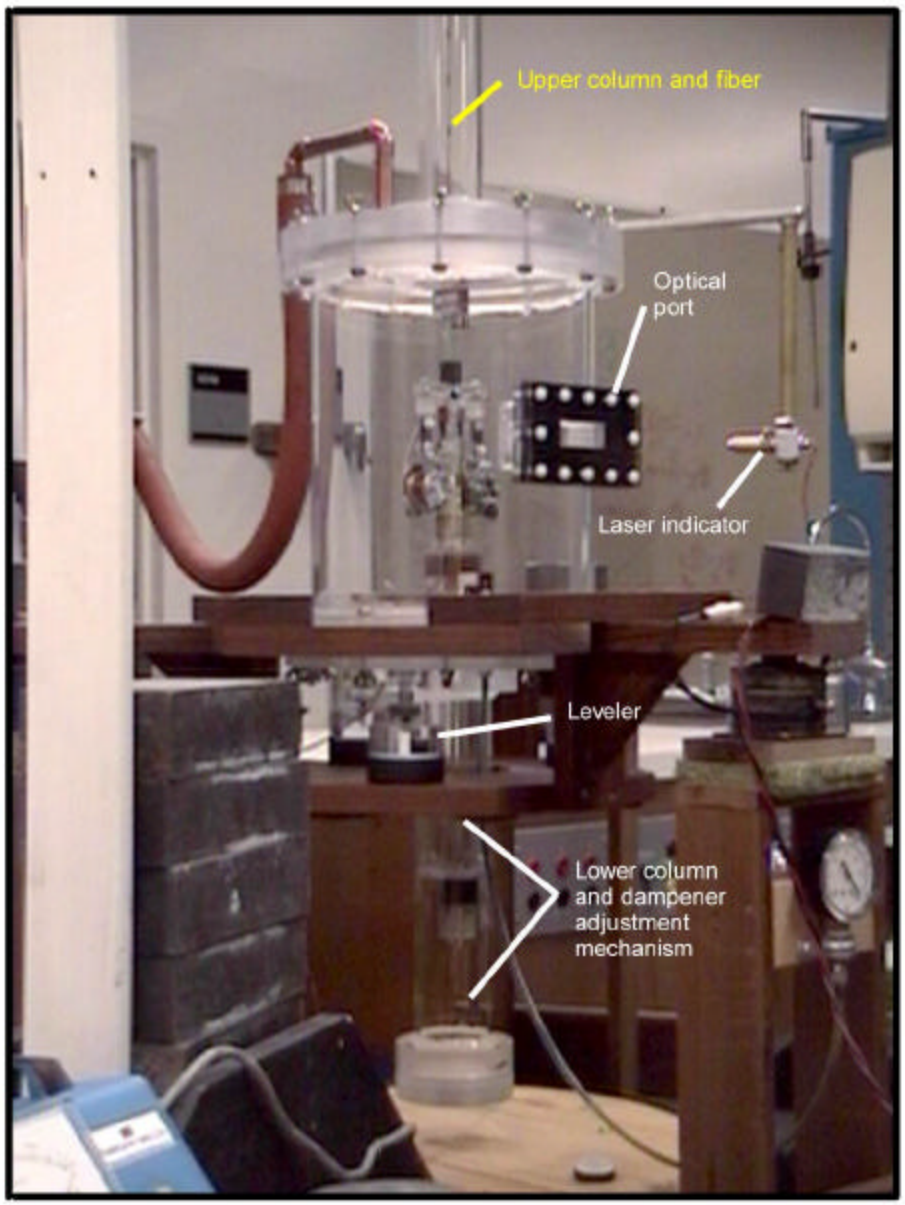
Upper column and fiber
Optical port
Laser indicator
Leveler
Lower column and dampener adjustment mechanism

Figure 8

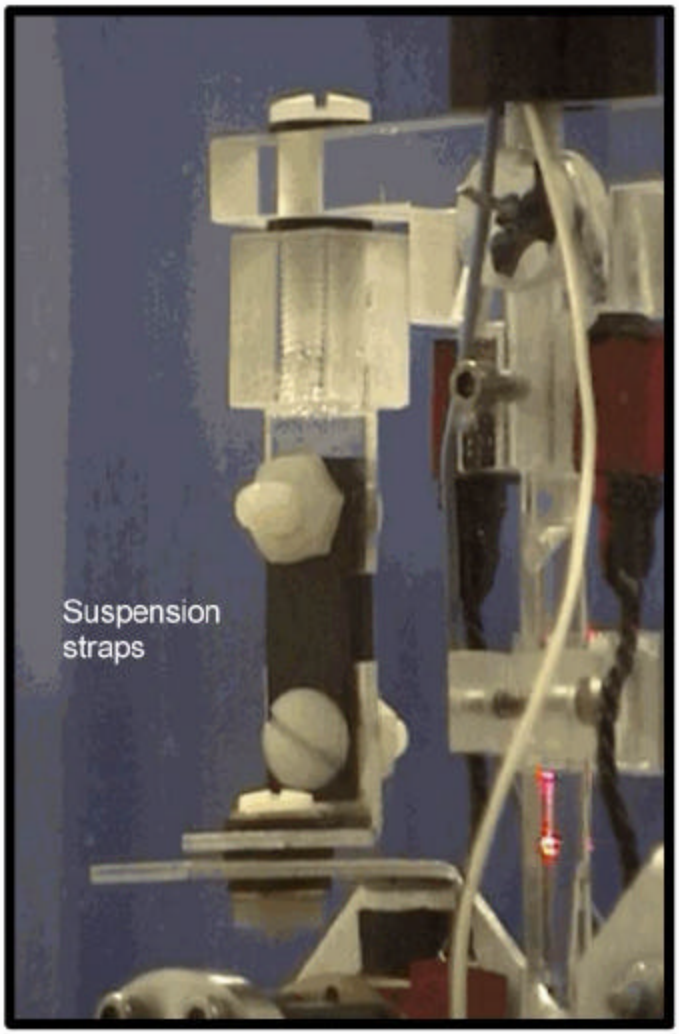

Figure 9

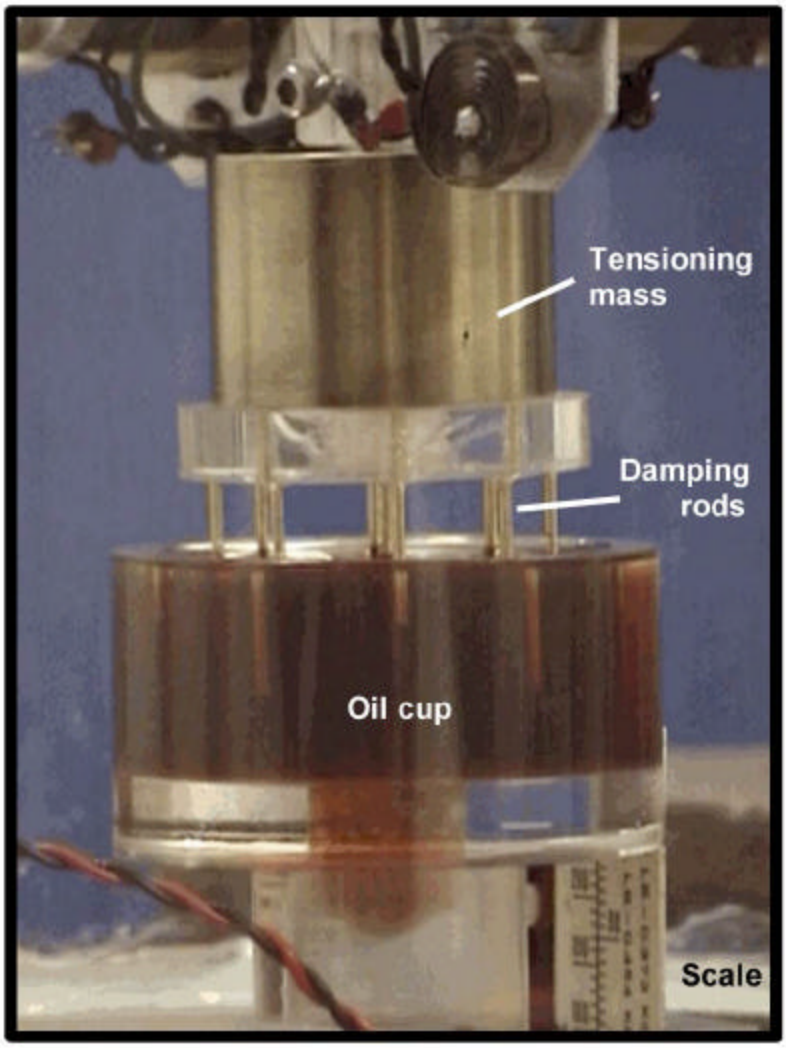

Figure 10

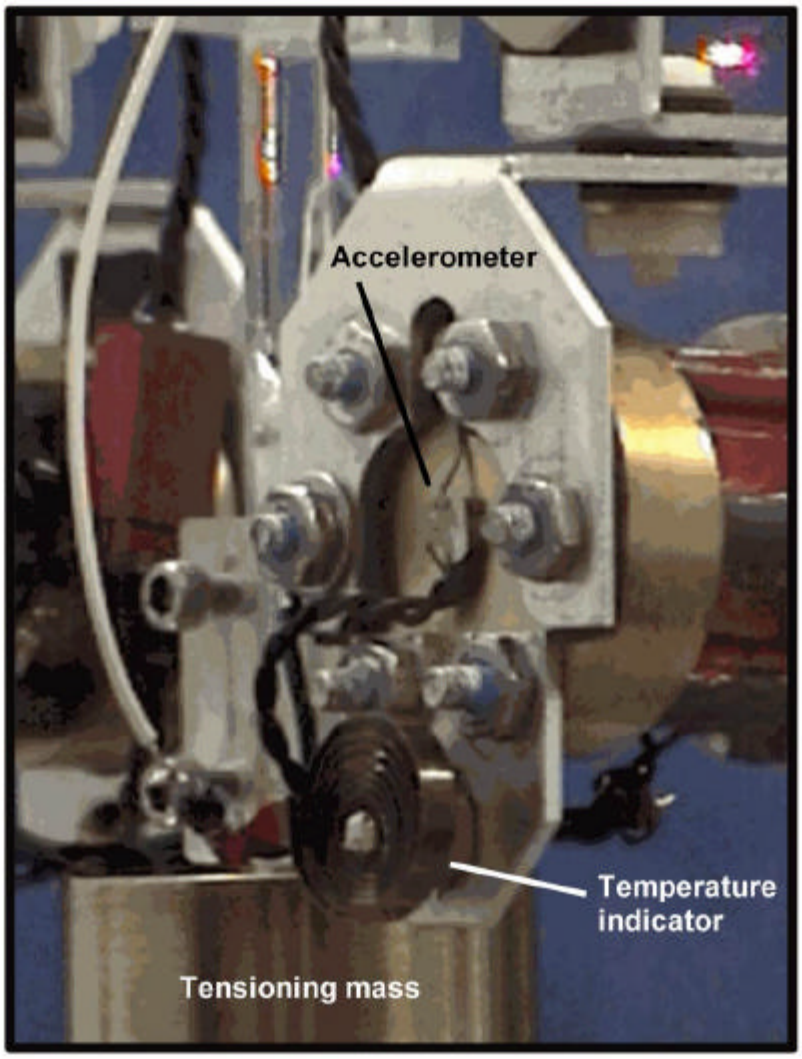
Accelerometer
Temperature indicator
Tensioning mass

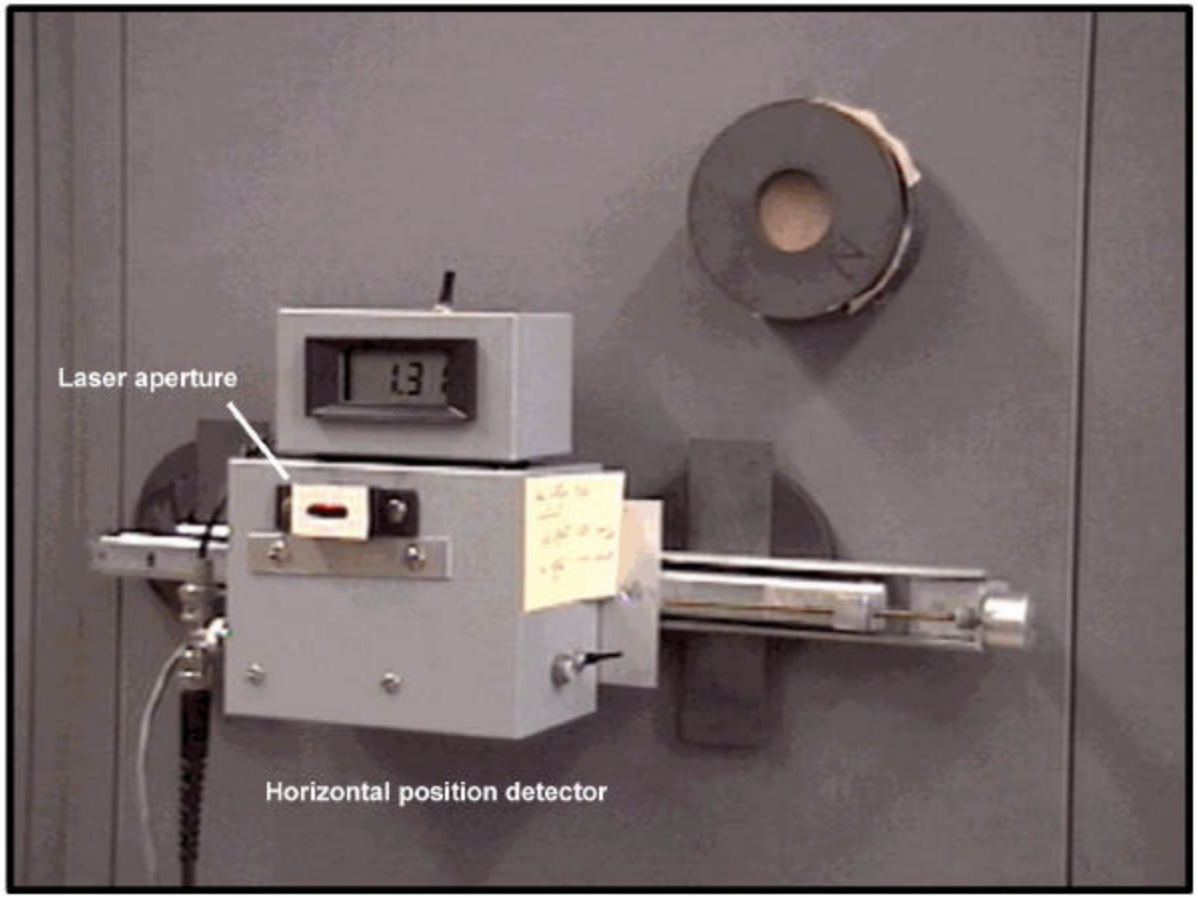

Figure 12

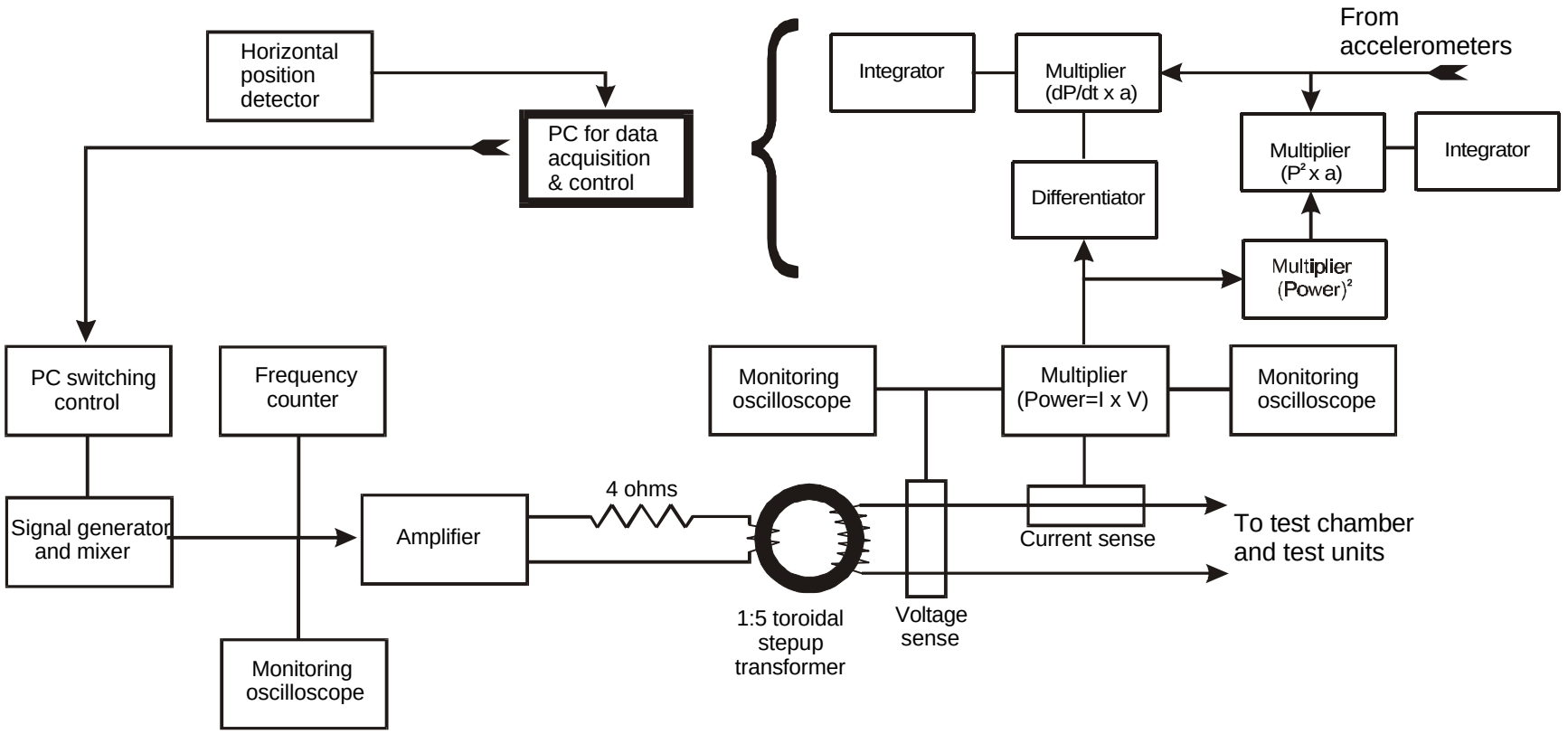
Horizontal position detector
PC for data acquisition & control
From accelerometers
Integrator
Multiplier (dP/dt x a)
Multiplier (P² x a)
Integrator
Differentiator
Multiplier (Power)²
PC switching control
Frequency counter
Monitoring oscilloscope
Multiplier (Power=I x V)
Monitoring oscilloscope
Signal generator and mixer
Amplifier
4 ohms
Current sense
To test chamber and test units
1:5 toroidal stepup transformer
Voltage sense
Monitoring oscilloscope

Figure 13

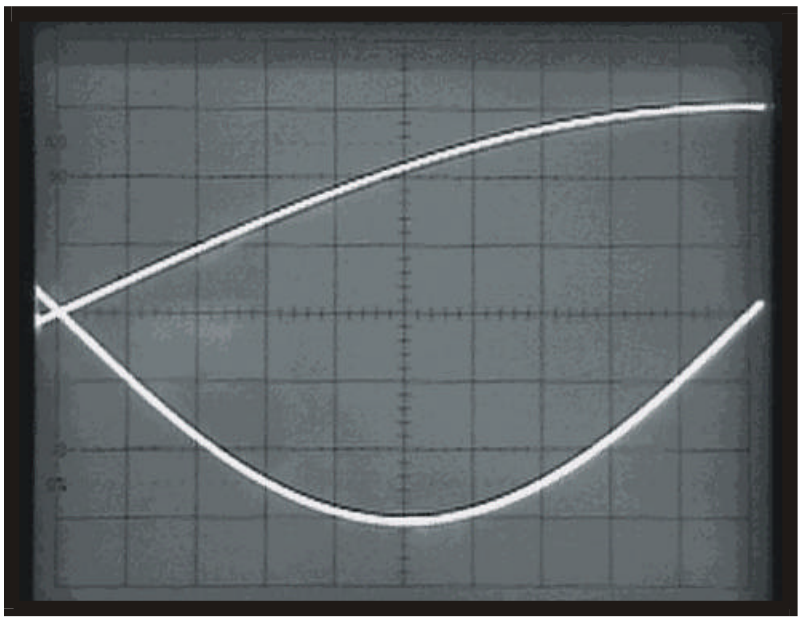

Figure 14. Omega and two omega base waveforms prior to mixing.

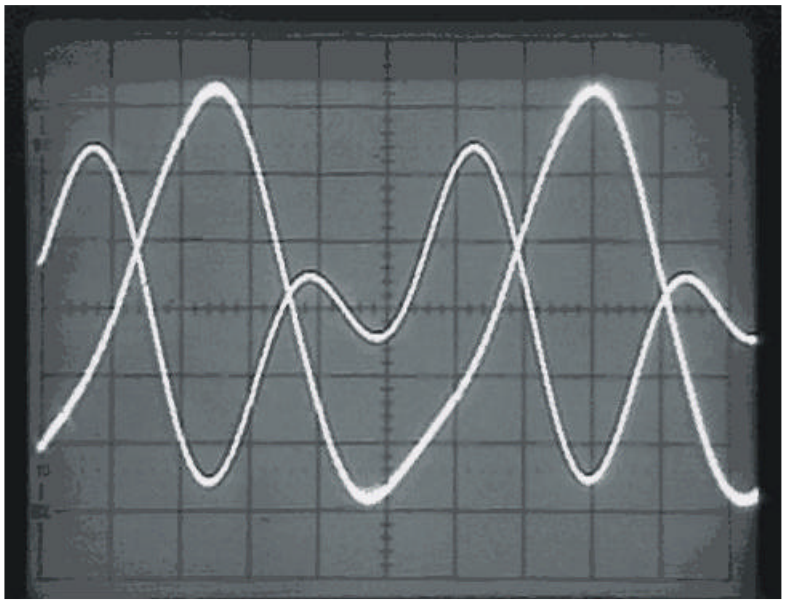

Figure 15. Mixed waveform and actual waveform as delivered to test units.

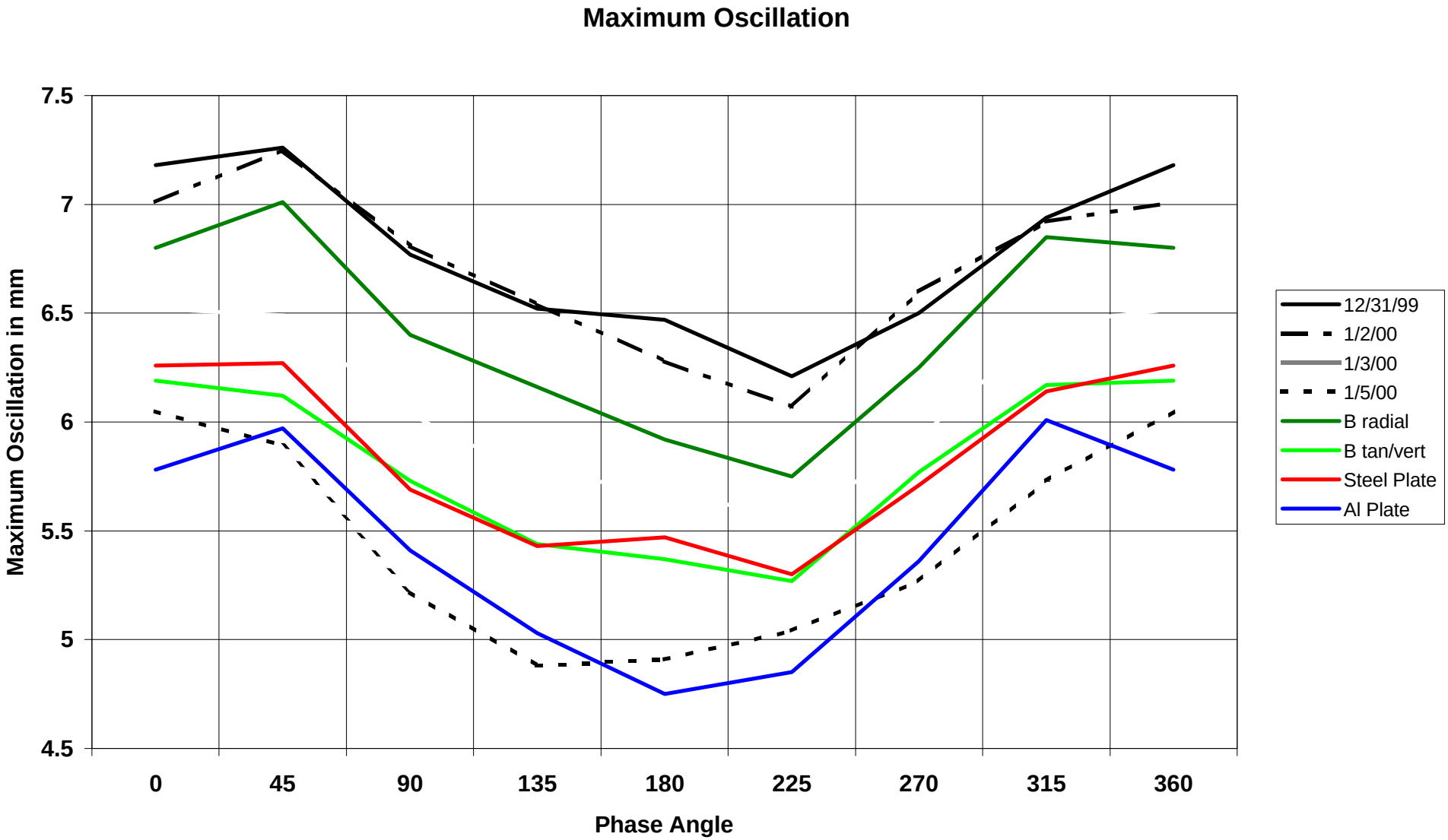
Maximum Oscillation
Maximum Oscillation in mm
7.5
7
6.5
6
5.5
5
4.5
0
45
90
135
180
225
270
315
360
Phase Angle
12/31/99
1/2/00
1/3/00
1/5/00
B radial
B tan/vert
Steel Plate
Al Plate

Figure 16

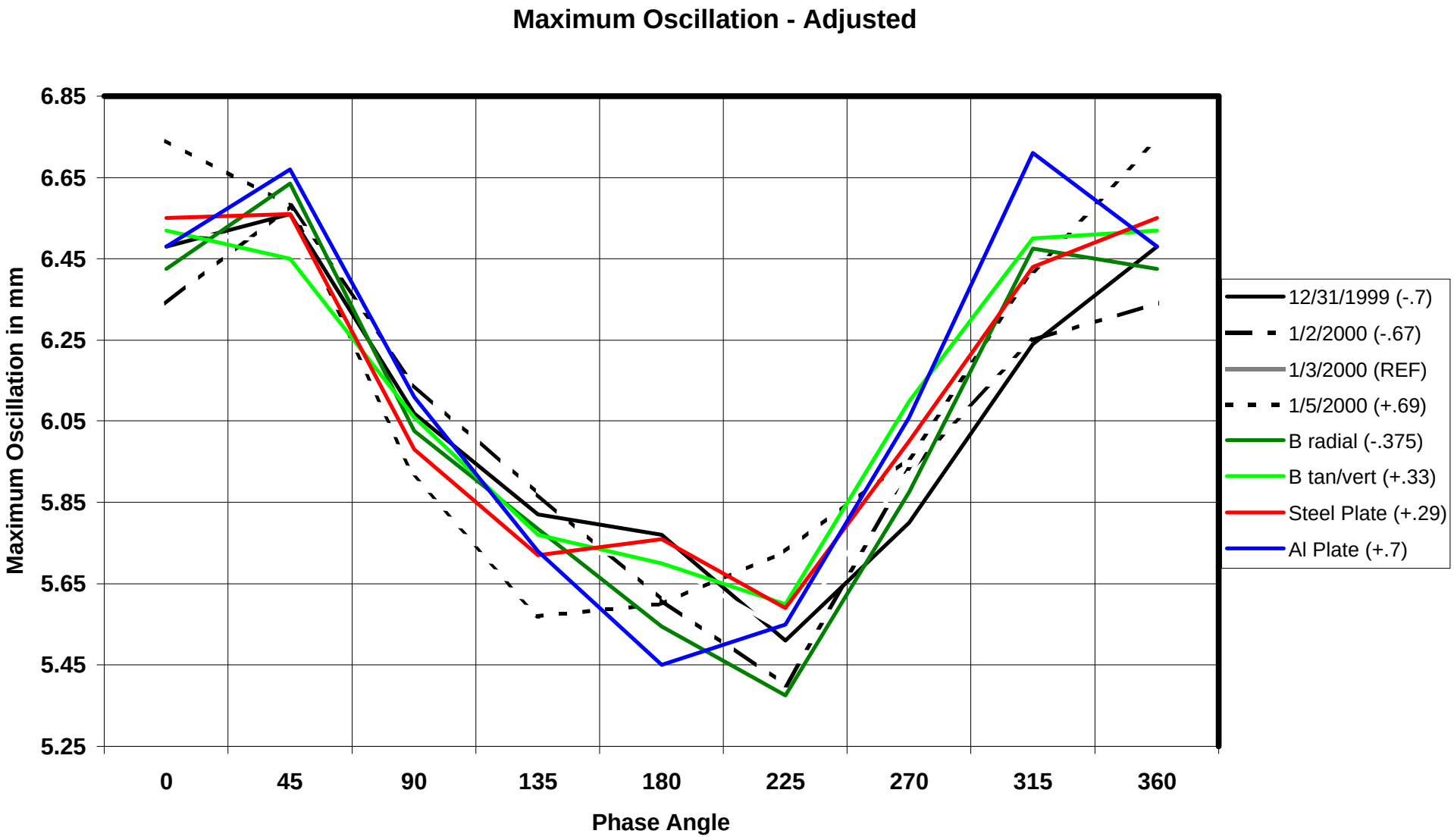
Maximum Oscillation - Adjusted
Maximum Oscillation in mm
6.85
6.65
6.45
6.25
6.05
5.85
5.65
5.45
5.25
0
45
90
135
180
225
270
315
360
Phase Angle
12/31/1999 (-.7)
1/2/2000 (-.67)
1/3/2000 (REF)
1/5/2000 (+.69)
B radial (-.375)
B tan/vert (+.33)
Steel Plate (+.29)
Al Plate (+.7)

Figure 17

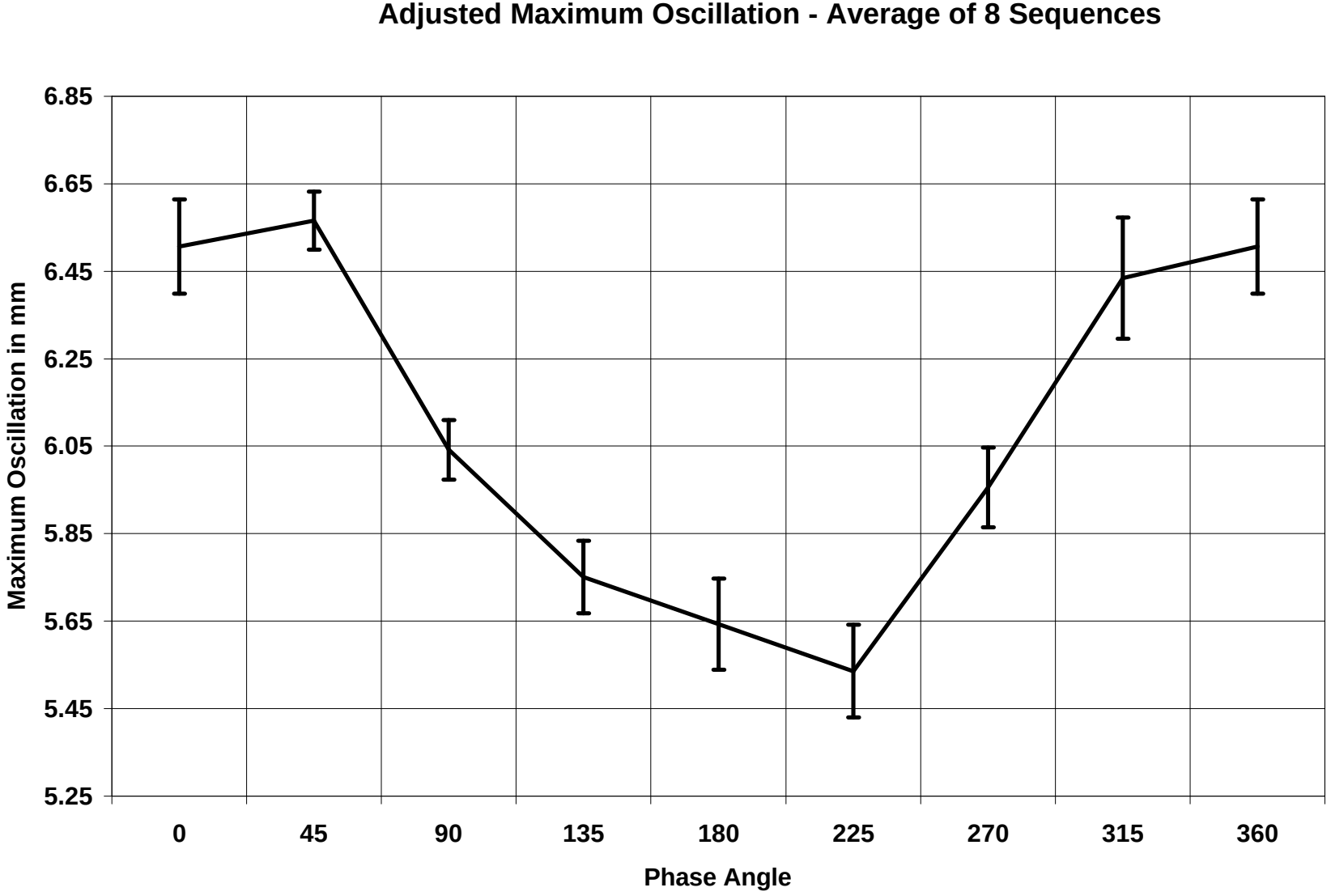
Adjusted Maximum Oscillation - Average of 8 Sequences
Maximum Oscillation in mm
6.85
6.65
6.45
6.25
6.05
5.85
5.65
5.45
5.25
0
45
90
135
180
225
270
315
360
Phase Angle

Figure 18

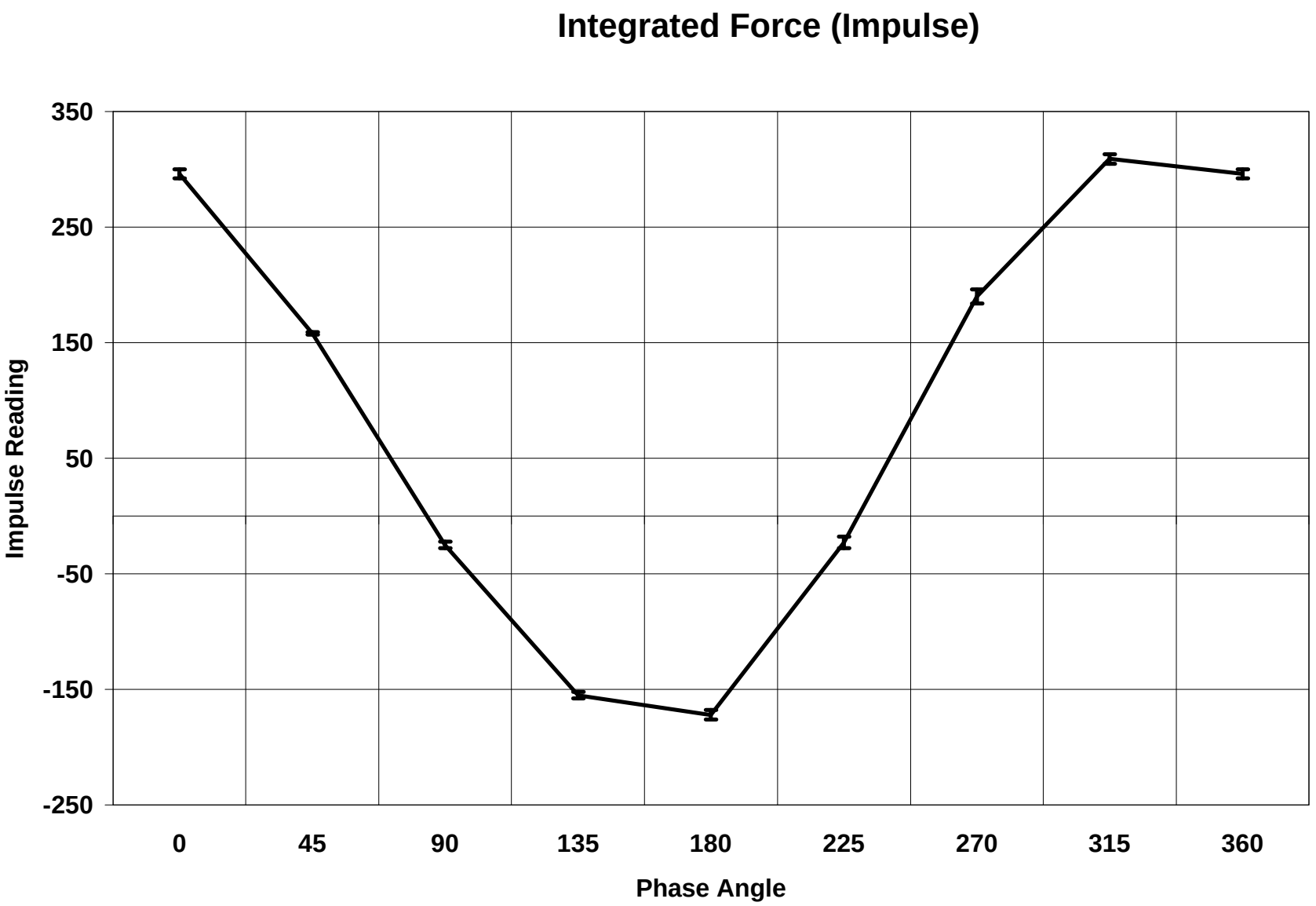
Integrated Force (Impulse)
350
250
150
50
-50
-150
-250
Impulse Reading
0
45
90
135
180
225
270
315
360
Phase Angle

Figure 19

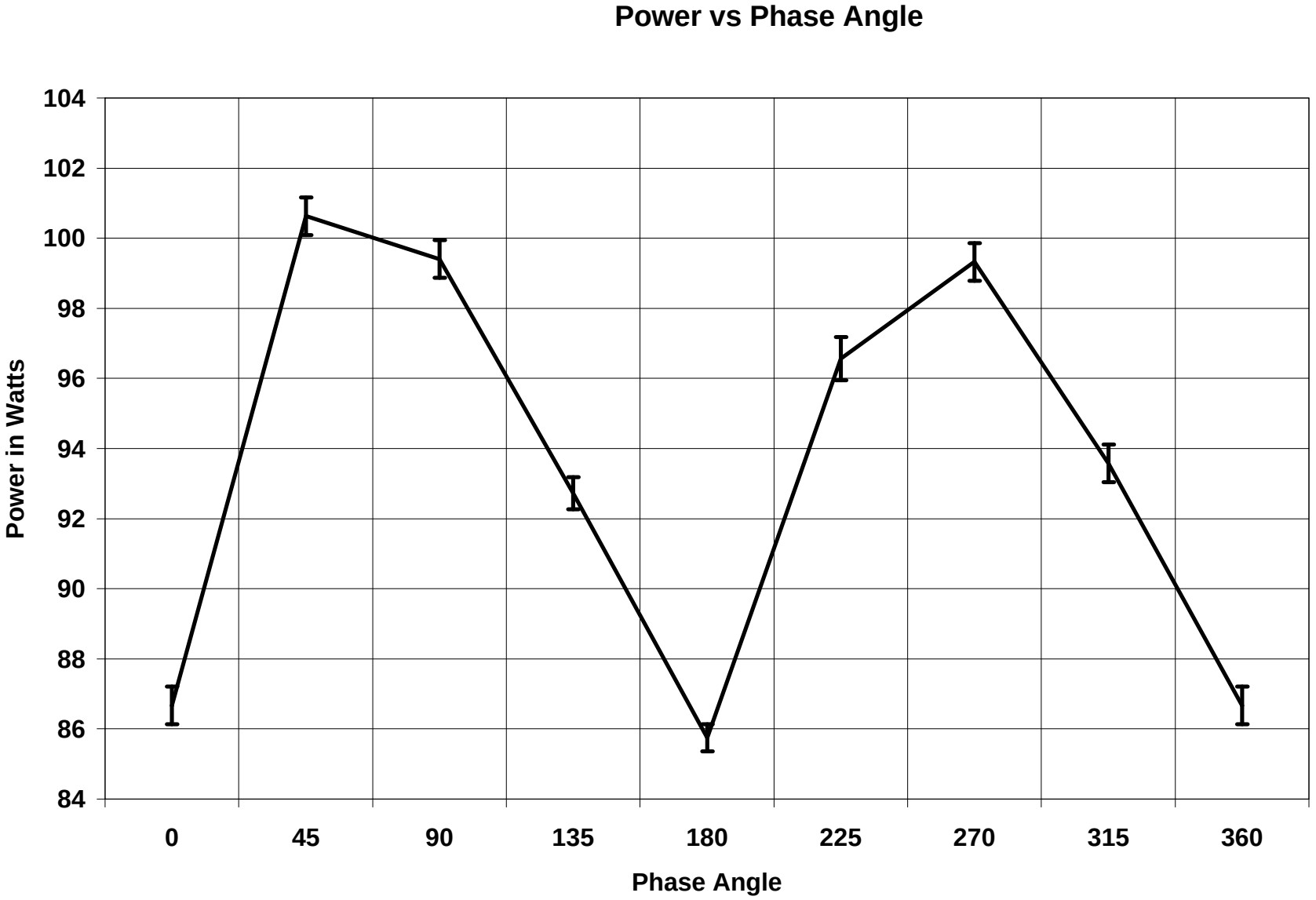
Power vs Phase Angle
104
102
100
98
96
94
92
90
88
86
84
Power in Watts
0
45
90
135
180
225
270
315
360
Phase Angle

Figure 20

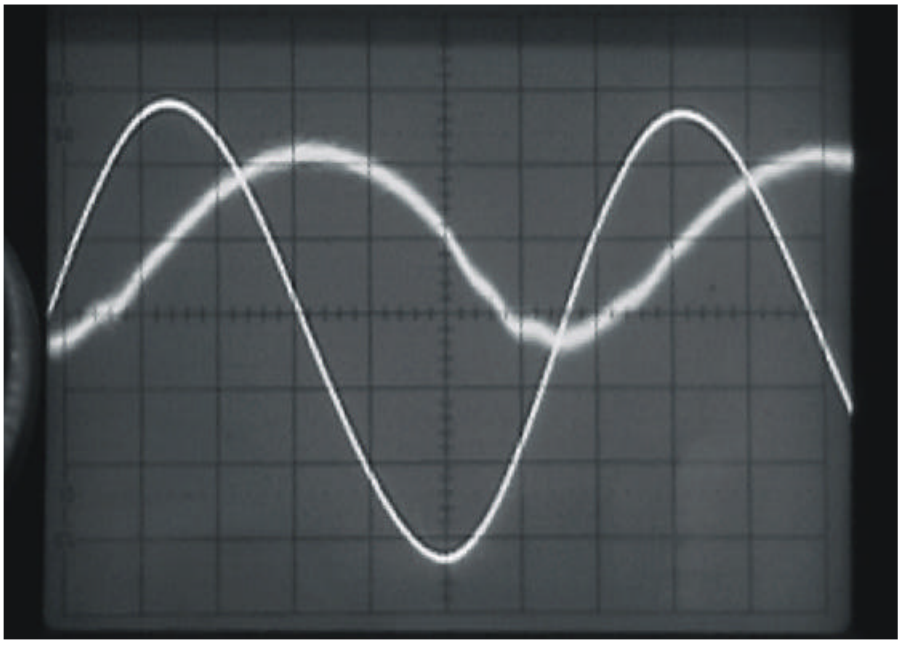

Figure 21. Power and dP/dt waveforms for pure sine wave driving signal.

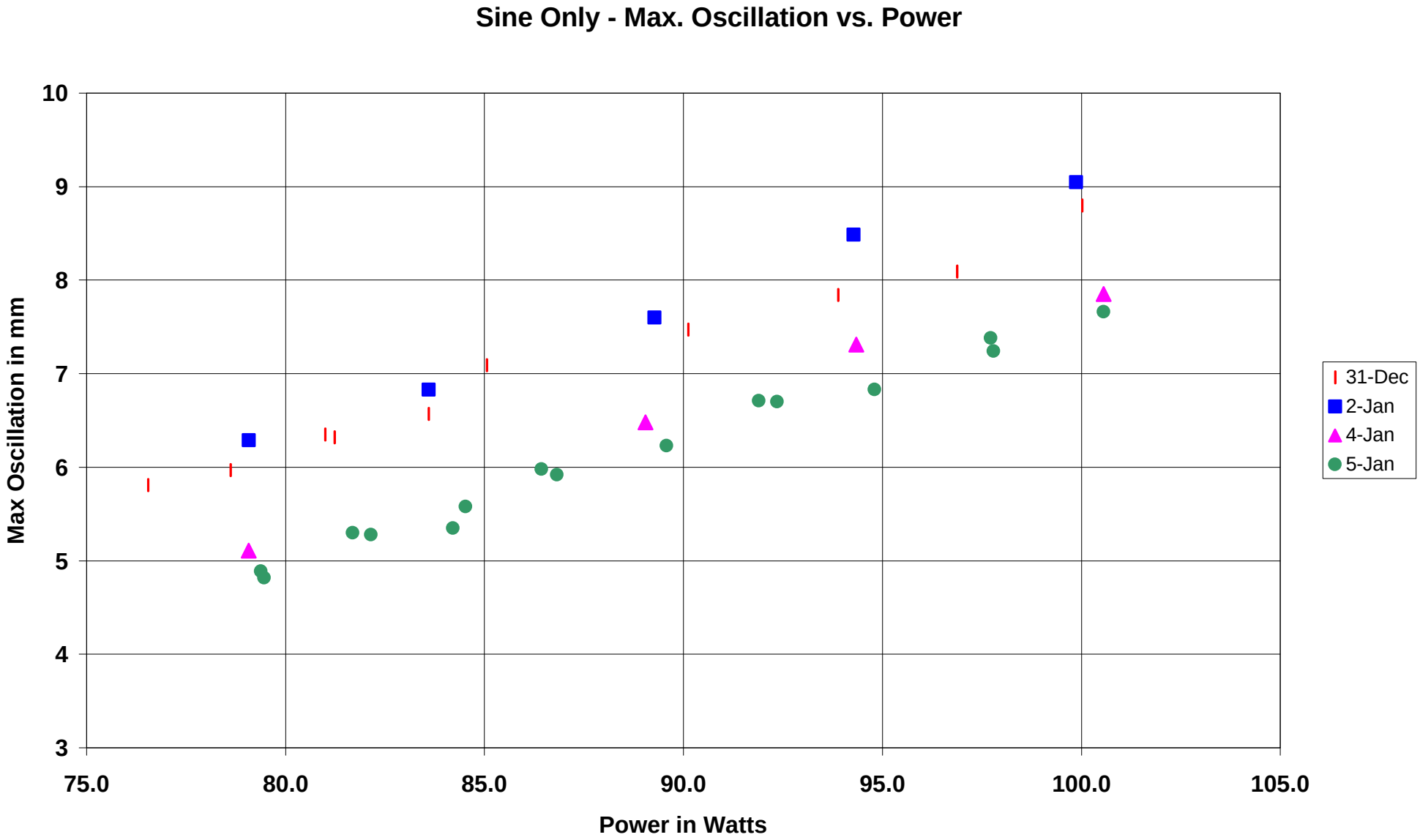
Sine Only - Max. Oscillation vs. Power
Max Oscillation in mm
10
9
8
7
6
5
4
3
75.0
80.0
85.0
90.0
95.0
100.0
105.0
Power in Watts
31-Dec
2-Jan
4-Jan
5-Jan

Figure 22

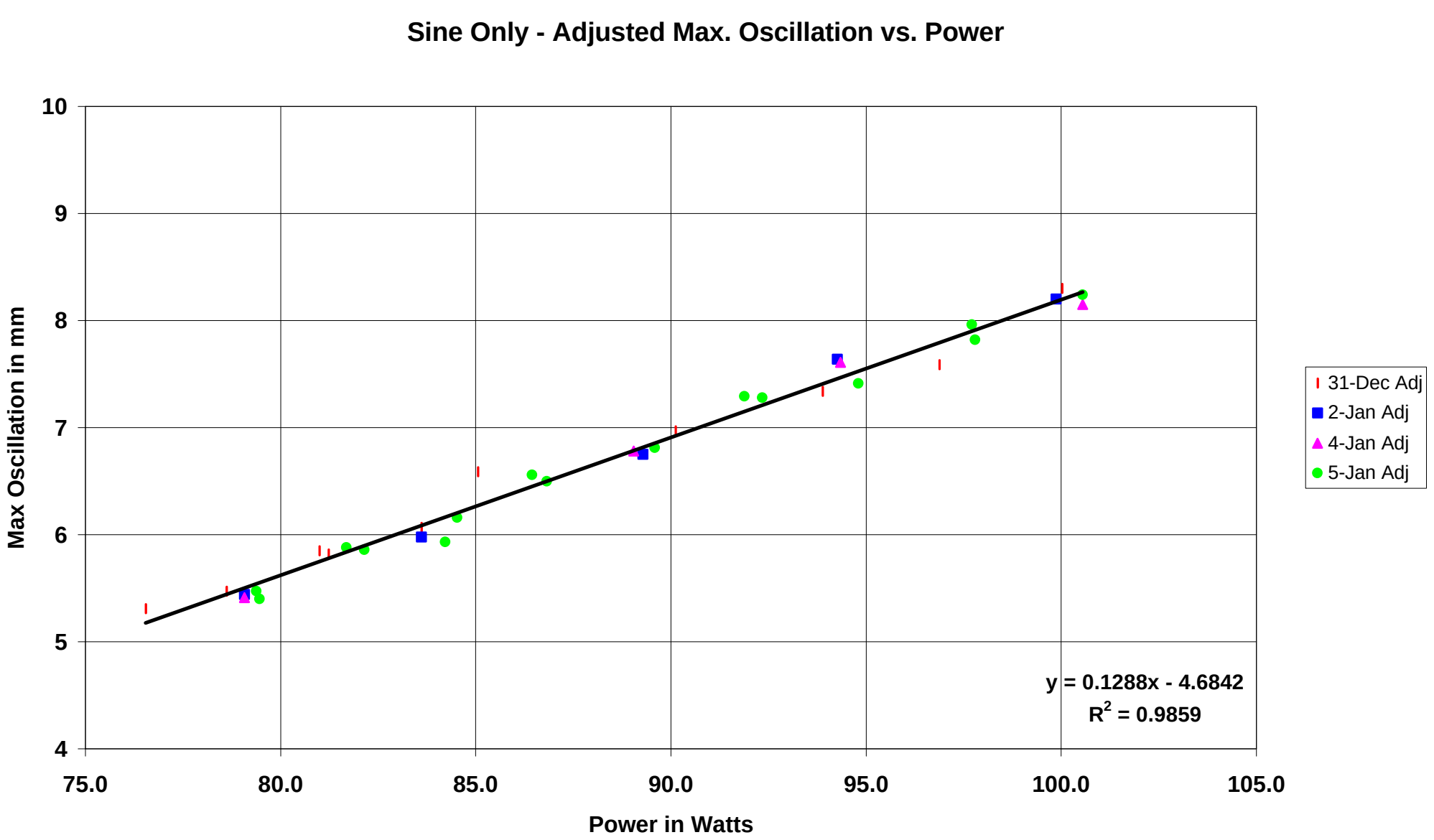
Sine Only - Adjusted Max. Oscillation vs. Power
Max Oscillation in mm
10
9
8
7
6
5
4
75.0
80.0
85.0
90.0
95.0
100.0
105.0
Power in Watts
y = 0.1288x - 4.6842
R2 = 0.9859
31-Dec Adj
2-Jan Adj
4-Jan Adj
5-Jan Adj

Figure 23

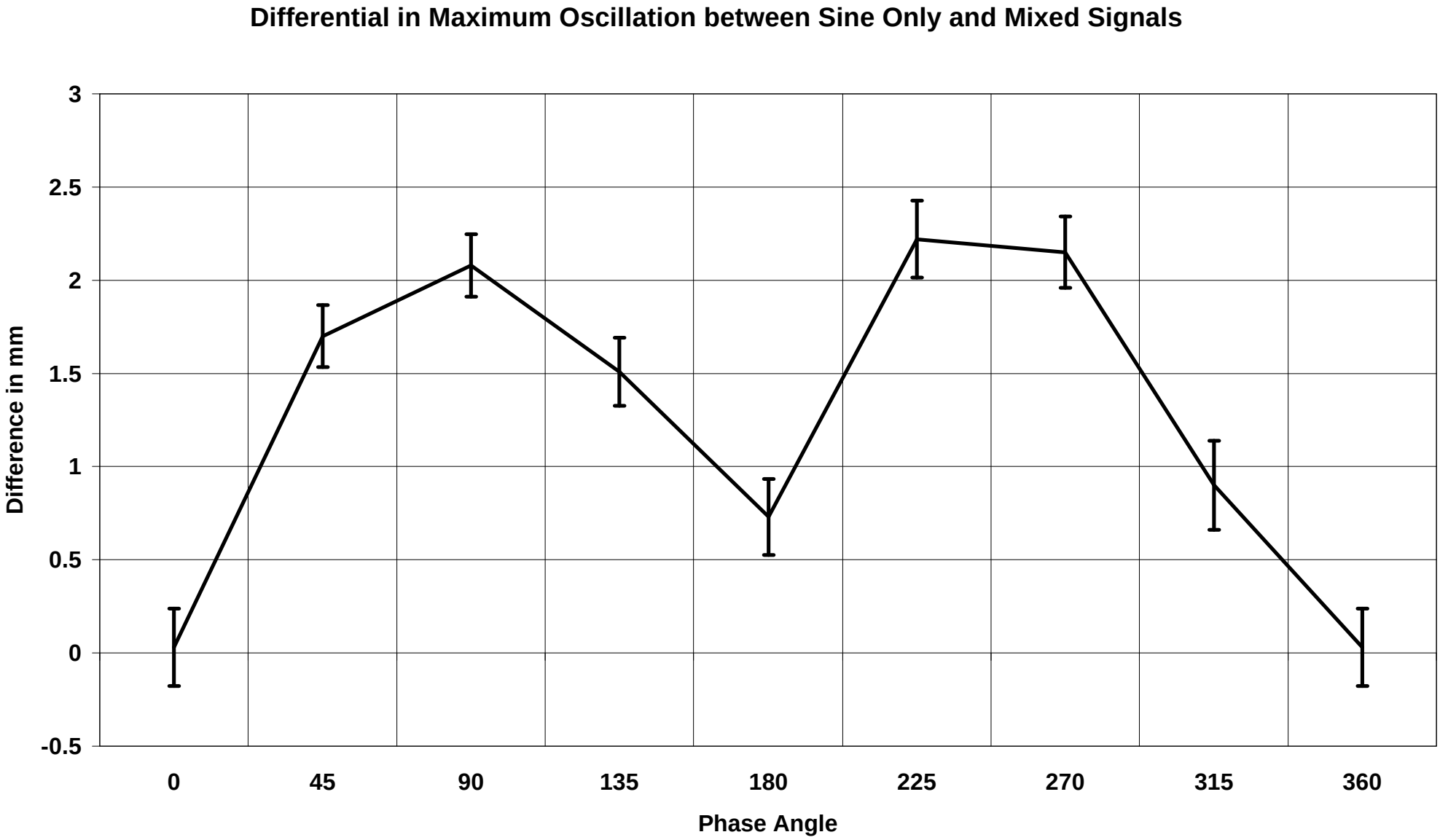
Differential in Maximum Oscillation between Sine Only and Mixed Signals
Difference in mm
3
2.5
2
1.5
1
0.5
0
-0.5
0
45
90
135
180
225
270
315
360
Phase Angle

Figure 24

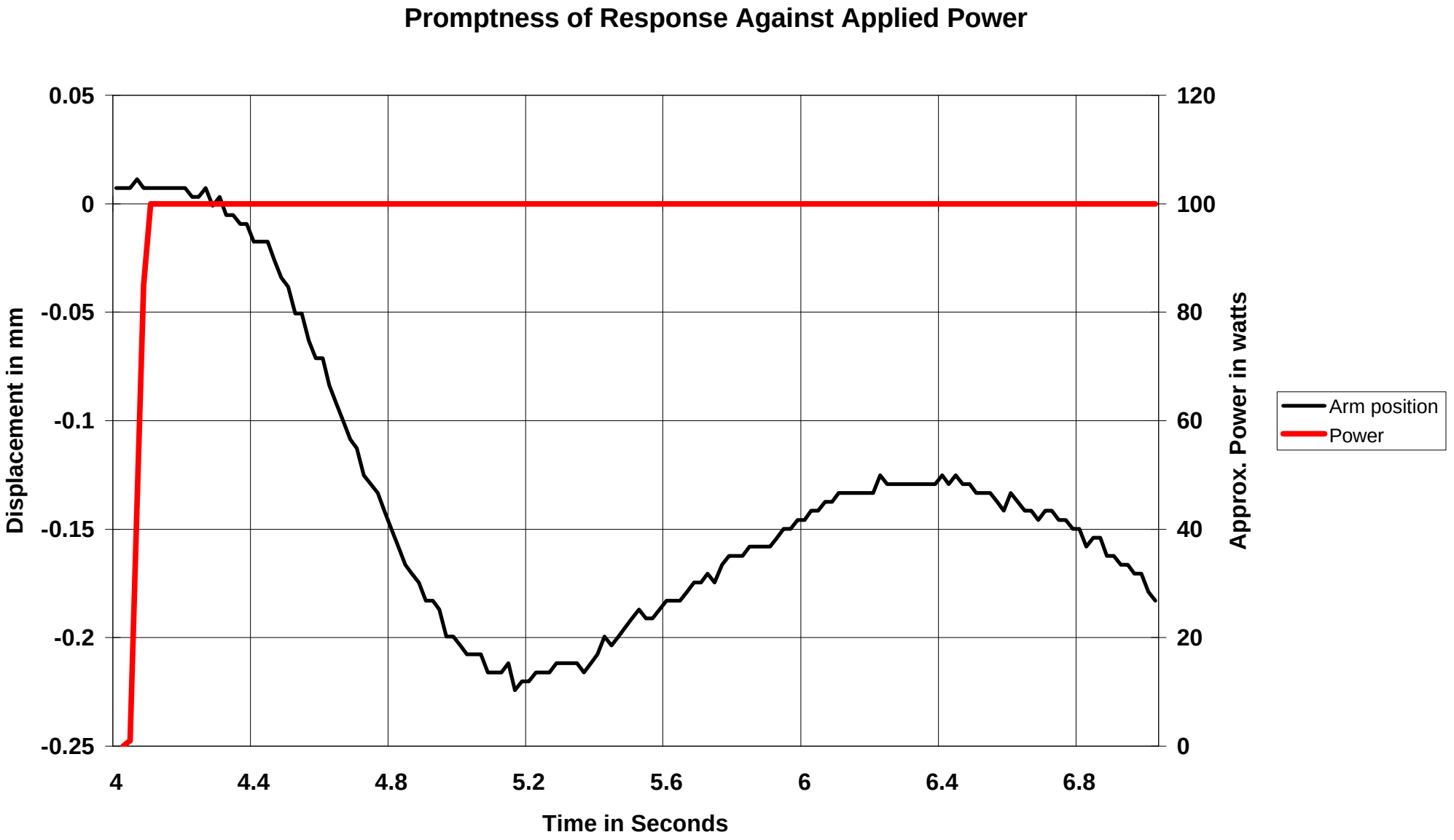
Promptness of Response Against Applied Power
0.05
0
-0.05
-0.1
-0.15
-0.2
-0.25
Displacement in mm
120
100
80
60
40
20
0
Approx. Power in watts
4
4.4
4.8
5.2
5.6
6
6.4
6.8
Time in Seconds
Arm position
Power

Figure 25

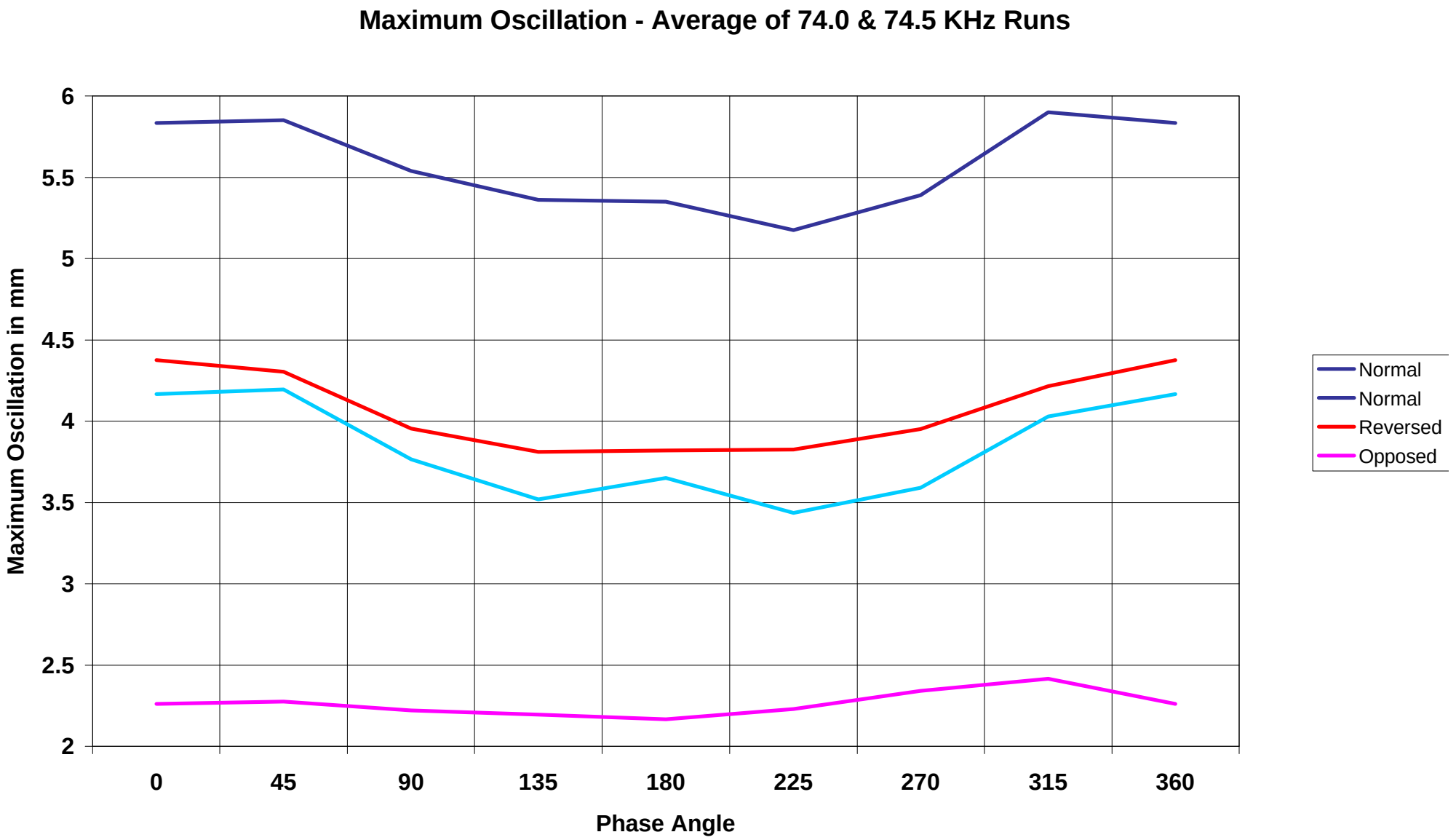
Maximum Oscillation - Average of 74.0 & 74.5 KHz Runs
Maximum Oscillation in mm
6
5.5
5
4.5
4
3.5
3
2.5
2
0
45
90
135
180
225
270
315
360
Phase Angle
Normal
Normal
Reversed
Opposed

Figure 26

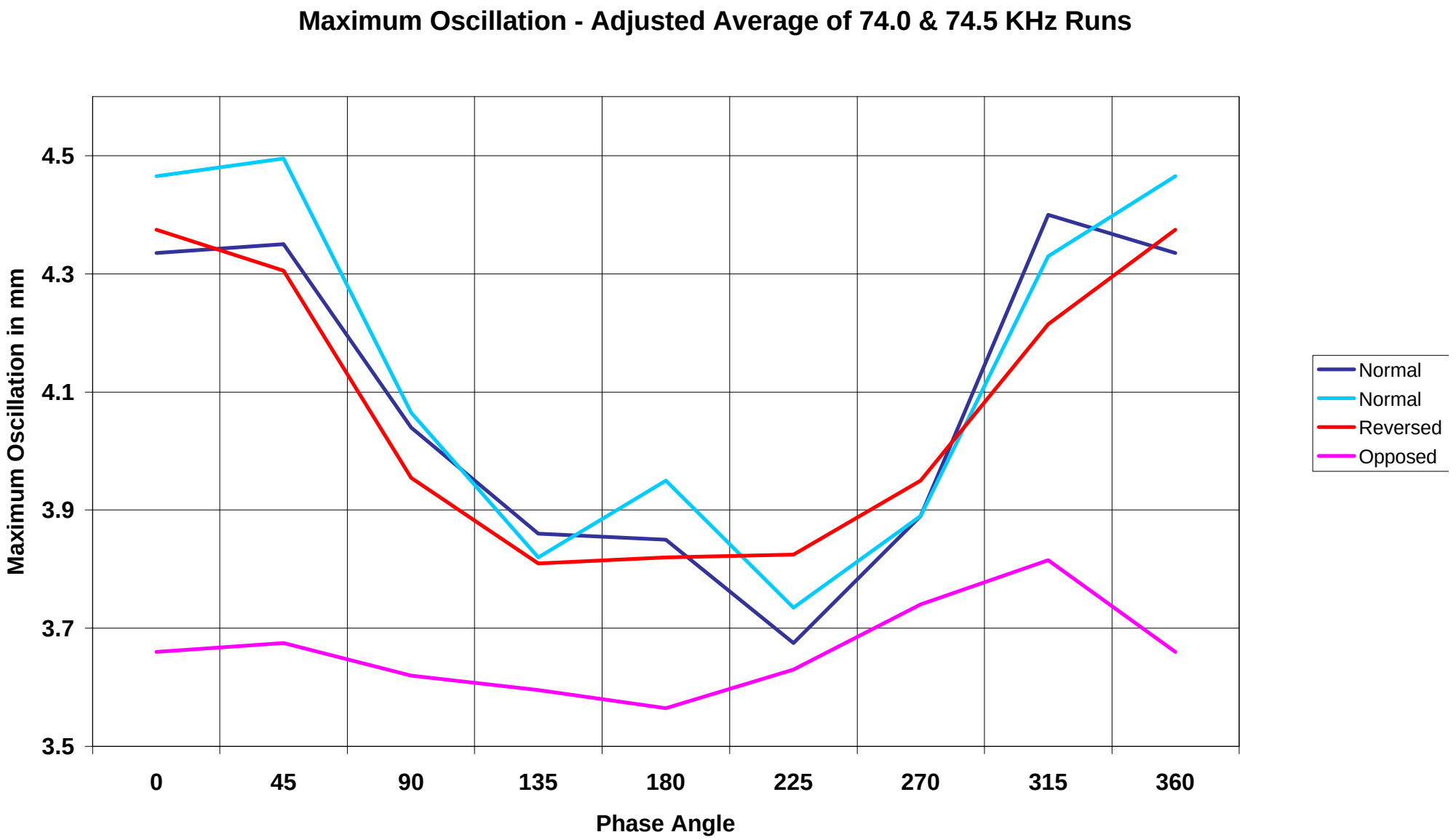
Maximum Oscillation - Adjusted Average of 74.0 & 74.5 KHz Runs
Maximum Oscillation in mm
4.5
4.3
4.1
3.9
3.7
3.5
0
45
90
135
180
225
270
315
360
Phase Angle
Normal
Normal
Reversed
Opposed

Figure 27

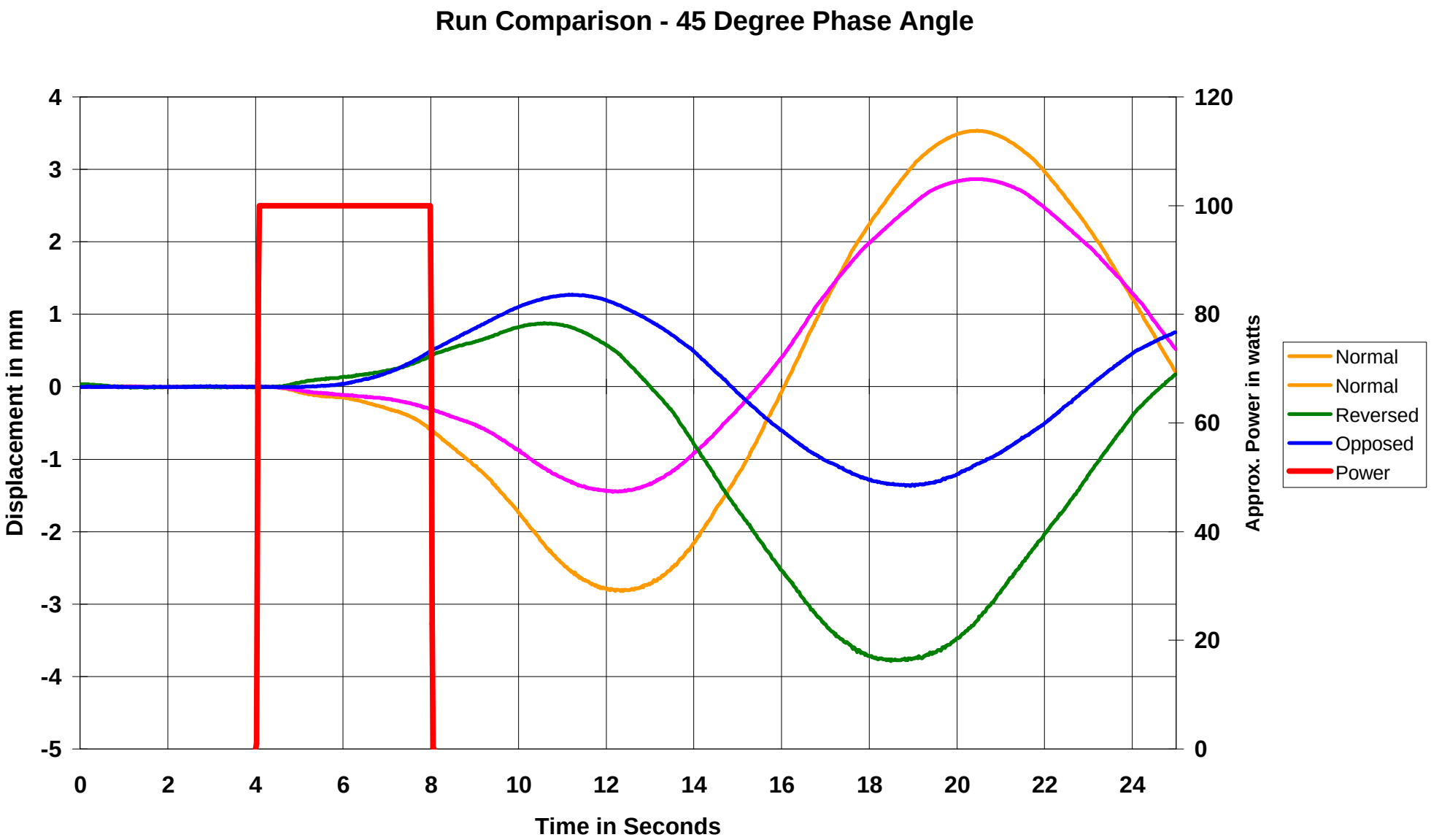
Run Comparison - 45 Degree Phase Angle
Displacement in mm
4
3
2
1
0
-1
-2
-3
-4
-5
Approx. Power in watts
120
100
80
60
40
20
0
0
2
4
6
8
10
12
14
16
18
20
22
24
Time in Seconds
Normal
Normal
Reversed
Opposed
Power

Figure 28

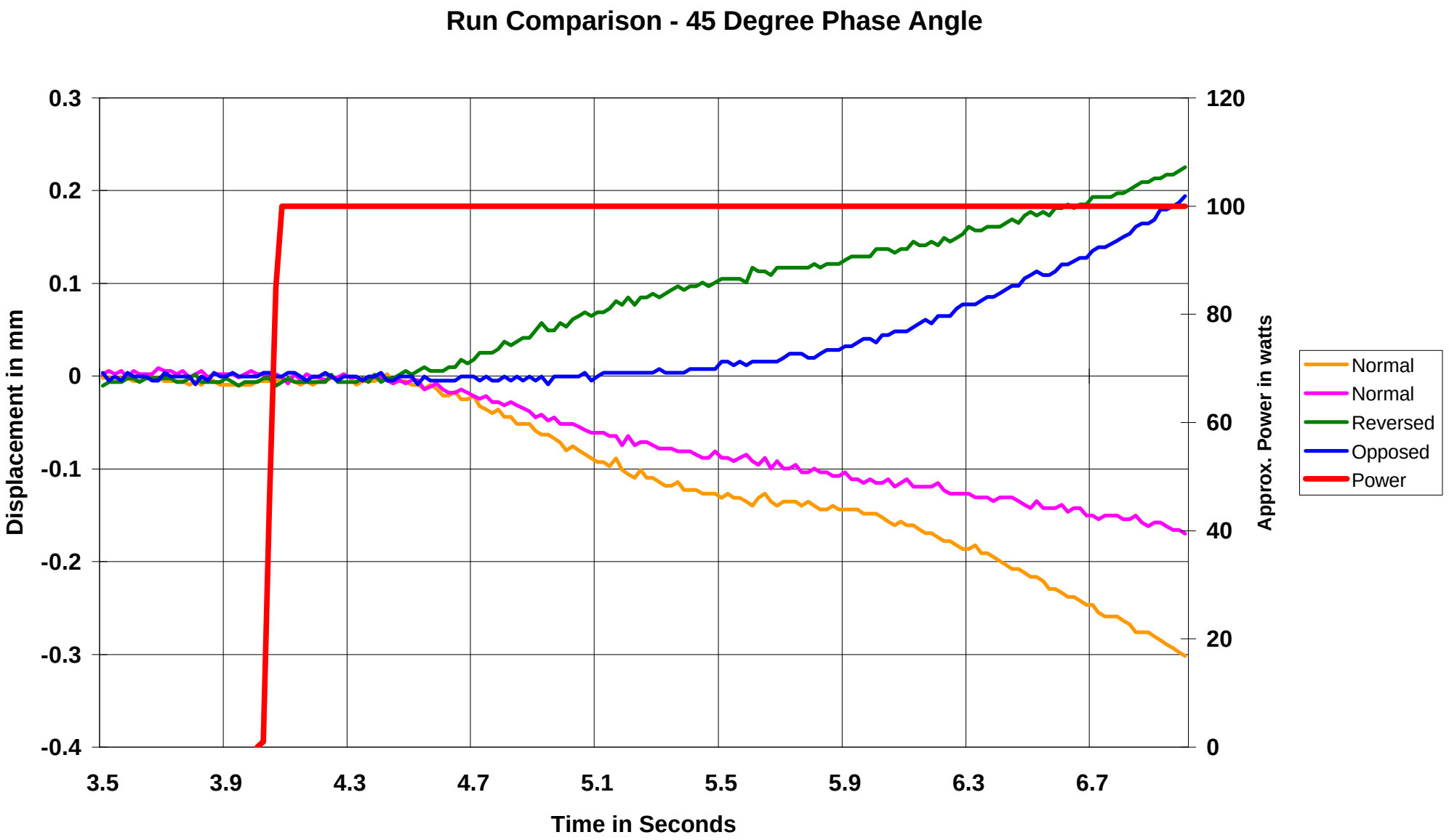
Run Comparison - 45 Degree Phase Angle
Displacement in mm
0.3
0.2
0.1
0
-0.1
-0.2
-0.3
-0.4
Approx. Power in watts
120
100
80
60
40
20
0
3.5
3.9
4.3
4.7
5.1
5.5
5.9
6.3
6.7
Time in Seconds
Normal
Normal
Reversed
Opposed
Power

Figure 29

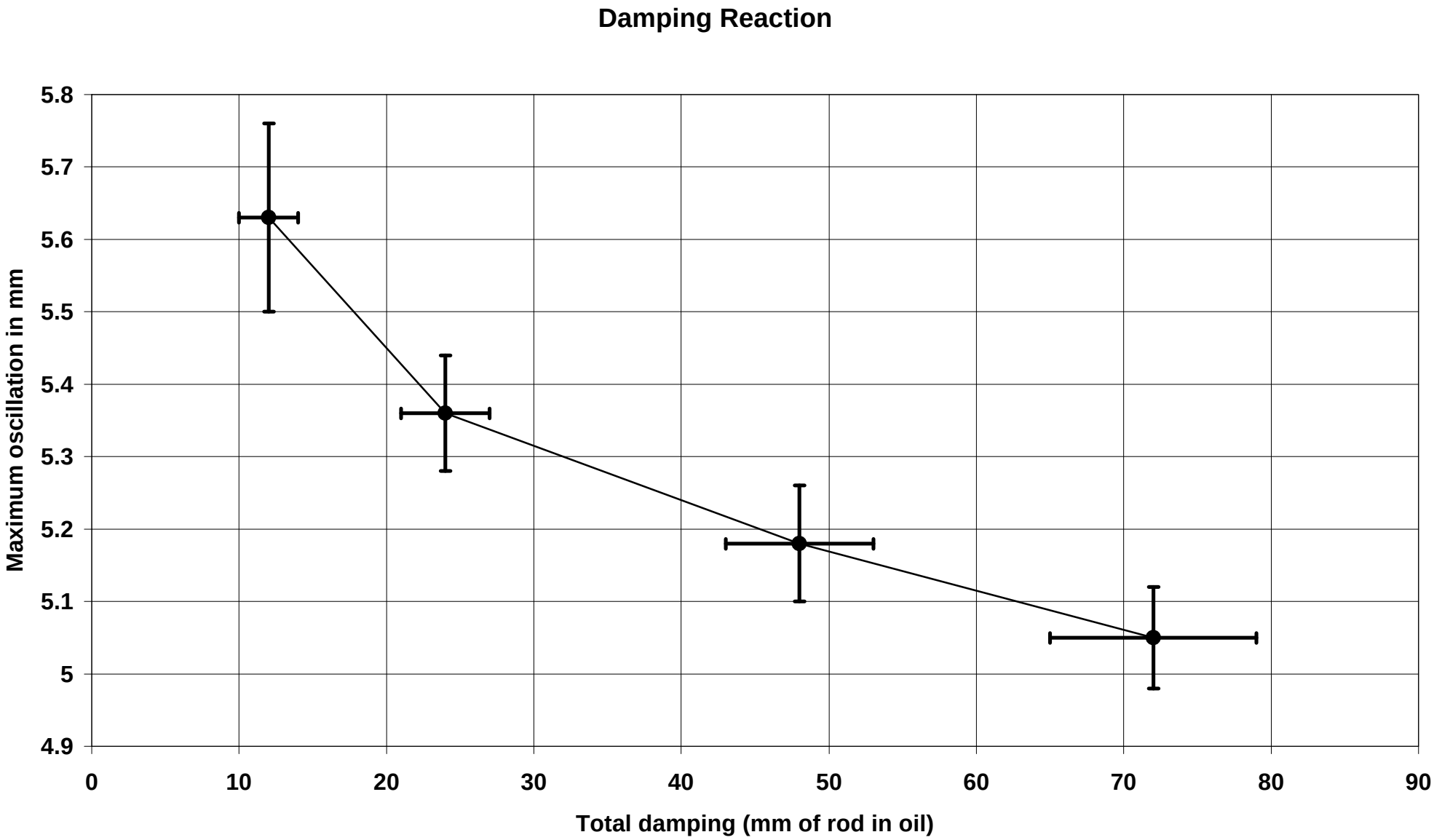
Damping Reaction
Maximum oscillation in mm
5.8
5.7
5.6
5.5
5.4
5.3
5.2
5.1
5
4.9
0
10
20
30
40
50
60
70
80
90
Total damping (mm of rod in oil)

Figure 30